2026-02-26

Theoretical Analysis of Electromagnetic Modes in Stratified Media

Islam, Md. Ariful

IUB

INDEPENDENT UNIVERSITY, BANGLADESH
Department of Physical Sciences

Theoretical Analysis of Electromagnetic Modes in Stratified Media

PHY499: Project in Physics

Report submitted in partial fulfillment of the requirements
for the degree of B.Sc. (Hons.) in Physics

Md. Ariful Islam
Student ID: 2211398

Under the supervision of **Prof. M. Arshad Momen**

26th February, 2026

Declaration

I, **Md. Ariful Islam**, declare that this thesis, titled "Theoretical Analysis of Electromagnetic Modes in Stratified Media," was completed as part of the Senior Project Course for my Bachelor's Degree at Independent University, Bangladesh and that no other sources or learning aids, other than those listed, have been used. Furthermore, I declare that I have acknowledged the work of others by providing detailed references of the said work.

Signature of the student: _____

Date: _____

Certification of The Report

The report titled "Theoretical Analysis of Electromagnetic Modes in Stratified Media," submitted by **Md. Ariful Islam**, ID: **2211398**, has been accepted as satisfactory in partial fulfillment of the requirement for the degree of B.Sc. (Hons.) in Physics on **26th February, 2026**.

Members of the Assessment Committee:

1. _____ Date: _____

Prof. M. Arshad Momen, PhD
(Supervisor)

2. _____ Date: _____

Rifat Ara Rouf, PhD
(Head of the Department of Physical Sciences)

3. _____ Date: _____

Prof. Mohammad Mostofa Kamal, PhD
(Member)

4. _____ Date: _____

Habib Bin Muzaffar, PhD
(Member)

5. _____ Date: _____

Jewel Kumar Ghosh, PhD
(Member)

Approval

The thesis titled "Theoretical Analysis of Electromagnetic Modes in Stratified Media," submitted by **Md. Ariful Islam**, ID: **2211398**, to the Department of Physical Sciences, School of Engineering, Technology and Sciences, Independent University, Bangladesh, has been accepted as satisfactory for the partial fulfillment of the requirements for the degree of Bachelor of Science in Physics and approved as to its style and contents.

_____ Date: _____

Signature of Supervisor

_____ Date: _____

Signature of the Head of the Department

_____ Date: _____

Signature of the Director GSRIR

Abstract

Electromagnetic wave propagation in stratified conducting media is a fundamental problem in underwater wireless communication and geophysical exploration. However, the accurate modeling of such environments is computationally challenging due to the highly oscillatory nature of the Bessel functions within the Sommerfeld integrals. This thesis develops a numerical method for analyzing electromagnetic modes in a three-layer model consisting of air, seawater, and seabed.

The Global Matrix Method (GMM) is employed to formulate the boundary value problem, allowing for the rigorous treatment of multiple reflections at the interfaces. To resolve the numerical instability associated with the Sommerfeld integrals, a custom integration solver was developed utilizing Romberg integration accelerated by the Shanks transformation (Wynn's ϵ-algorithm)[1]. This hybrid approach ensures stable convergence for the oscillatory integrands, overcoming the limitations of standard quadrature methods.

Using this solver, the electromagnetic field components generated by a submerged Horizontal Magnetic Dipole (HMD) were explicitly calculated. The results confirm the transition from direct wave dominance in the near-field to lateral wave propagation in the far-field, demonstrating the efficacy of the proposed method for modeling propagation in lossy stratified environments.

Keywords: Electromagnetic Modeling, Global Matrix Method, Stratified Media, Sommerfeld Integrals, Spectral Domain Analysis, Computational Physics.

Acknowledgements

First and foremost, I would like to express my deepest gratitude to the Almighty for granting me the strength, patience, and ability to complete this research work.

I am profoundly grateful to my supervisor, Prof. M. Arshad Momen, for his invaluable guidance, continuous encouragement, and deep insight throughout the course of this project. His expertise in electromagnetic theory and his patience in explaining the complex mathematical concepts were essential to the completion of this research.

I extend my sincere thanks to the Department of Physical Sciences at Independent University, Bangladesh (IUB), for providing the necessary academic resources and a stimulating learning environment. I am also grateful to the faculty members of the department of Physical Sciences for their support during my undergraduate studies.

A special thanks goes to my friends for the stimulating discussions and moral support that kept me motivated during the challenging phases of this research.

Finally, I am forever indebted to my parents and family. Their unconditional love, sacrifice, and belief in my potential have been my greatest source of inspiration. This work is dedicated to them.

Md. Ariful Islam
Dhaka, Bangladesh
February 2026

Contents

List of Figures

Chapter 1

Introduction

1.1 Background: Electromagnetic Waves in Marine Environments

The study of electromagnetic (EM) wave propagation in seawater is a cornerstone of modern oceanography, underwater navigation, and distinct communication systems used by submersibles. Unlike the atmosphere, where radio waves travel freely over vast distances, the ocean presents a uniquely hostile environment for wireless transmission.[2] Seawater is a highly conductive electrolyte, with conductivity values typically ranging from 3 to 5 S/m. When an electromagnetic wave enters this medium, the oscillating field induces ionic currents that dissipate energy as heat. This phenomenon leads to rapid signal attenuation, known as the "skin effect," which severely restricts the penetration depth of standard high-frequency radio signals to mere centimeters.

To circumvent this physical limitation, naval and scientific applications have historically turned to the lower end of the electromagnetic spectrum[3][4]. Extremely Low Frequency (ELF, 3–30 Hz) and Very Low Frequency (VLF, 3–30 kHz) waves possess wavelengths long enough to minimize attenuation, allowing them to penetrate to significant depths. For instance, a submerged Horizontal Magnetic Dipole (HMD) is often used as a standard model for underwater antennas[5] because magnetic fields are generally less affected by the medium's permittivity than electric fields. However, even at these low frequencies, the theoretical modeling of signal propagation remains a complex mathematical challenge.[6]

A significant limitation in many classical theoretical models is the oversimplification of the ocean itself. Early research often treated the sea as a homogeneous, isotropic half-space—essentially a single, uniform block of saltwater with constant conductivity and permittivity. While this assumption allows for convenient analytical solutions (often involving Sommerfeld integrals[7]), it fails to capture the dynamic

reality of the marine environment. In reality, the ocean is stratified. Factors such as solar heating, salinity gradients from freshwater runoff, and pressure variations create distinct layers within the water column, known as the thermocline and halocline.

Recent research, including the work of Wang et al. (2024)[8] and Goode[9], has demonstrated that these vertical variations in electromagnetic parameters cannot be ignored. The propagation of a wave in a non-homogeneous medium is subject to reflection and refraction at every interface between these layers. This can lead to complex interference patterns and "ducting" effects, where the signal is trapped in a specific layer, carrying it further than predicted by homogeneous models. Therefore, accurate prediction of the electromagnetic field requires a multi-layered model (N-layered media) that accounts for these discrete changes in material properties.[10]

This thesis addresses these challenges by employing the Direct Global Matrix Method. Unlike recursive methods, which propagate error and can become numerically unstable when dealing with thick or highly conductive layers, the Global Matrix Method solves for the boundary coefficients of all layers simultaneously. By combining this stable formulation with robust numerical integration techniques—specifically the Romberg method—this work aims to provide a precise simulation of the electromagnetic field generated by a source submerged in a realistic, non-homogeneous ocean environment.

1.2 Problem Statement: The Non-Homogeneous Nature of Seawater

A fundamental challenge in underwater electromagnetics lies in the accurate representation of the propagation medium. Classical models often simplify the ocean as a "half-space" with uniform electromagnetic properties—assuming constant conductivity (σ), permittivity (ϵ), and permeability (μ) throughout the entire water column. While this assumption facilitates analytical solutions, it contradicts oceanographic reality.

In a realistic marine environment, these parameters are not constant; they exhibit significant spatial variation, particularly with depth. The conductivity of seawater is primarily a function of its salinity (S) and temperature (T), both of which vary due to solar heating, evaporation, freshwater influx, and ocean currents.[11]

1. **Temperature Gradients (Thermocline):** The upper layer of the ocean (mixed layer) is typically warmer, while temperature decreases rapidly in the thermocline layer before stabilizing in the deep ocean. Since ionic mobility increases with temperature, conductivity drops significantly as depth increases.

2. **Salinity Gradients (Halocline):** Variations in salt concentration, driven by surface evaporation or river discharge, create distinct salinity profiles that further modulate conductivity.

3. **Pressure Effects:** At extreme depths, hydrostatic pressure also influences the dielectric properties of water, although to a lesser extent than temperature and salinity.

Because of these variations, seawater acts as a non-homogeneous, stratified medium. An electromagnetic wave propagating through such a medium encounters continuous changes in impedance. Treating the ocean as a single homogeneous block neglects the localized reflections and refractions that occur at these gradient interfaces. This oversight can lead to substantial errors in predicting the electric field intensity and phase, especially for sources submerged within the thermocline or halocline layers. Therefore, to achieve high-fidelity modeling, the ocean must be discretized into N horizontal layers, each with distinct, constant electromagnetic parameters, thereby approximating the continuous vertical profile.

1.3 Existing Methods and Their Limitations

The problem of electromagnetic wave propagation in stratified media has been a subject of extensive research for over a century. Various mathematical and numerical techniques have been developed to solve the vector Helmholtz equation in layered environments. These methods generally fall into two categories: semi-analytical integral methods and full-wave numerical simulations. While each approach has its merits, they also possess significant limitations when applied to the complex, highly conductive, and multi-layered environment of the ocean.

1.3.1 Semi-Analytical Approximations

The Homogeneous Half-Space

The earliest and most fundamental approach, pioneered by Arnold Sommerfeld in 1909, treats the ocean as a single, semi-infinite homogeneous half-space bounded by air above and the seabed below [14, 15]. This model simplifies the problem significantly, reducing the solution to a set of canonical integrals known as Sommerfeld Integrals.

While analytically elegant, the homogeneous half-space model suffers from a critical deficiency: it cannot account for the vertical stratification of seawater. As discussed in Section 1.2, the conductivity of seawater varies with depth due to the thermocline and halocline. The homogeneous model averages these parameters into a

single bulk value, thereby neglecting the localized reflections and guided wave modes (ducting) that occur at internal layer interfaces. Consequently, this method often fails to accurately predict field intensity at specific depths where local conductivity differs significantly from the average.

Recursive Methods: The Transmission Line Approach

To address stratification, researchers developed multi-layered models solved via recursive algorithms. The most common of these is the Transmission Line (TL) Method or the Generalized Reflection Coefficient Method. This approach draws an analogy between plane wave propagation in layers and voltage/current propagation on a transmission line.

In this method, the solution is built layer-by-layer. Starting from the bottom-most layer (the seabed), a local reflection coefficient is calculated and then "propagated" upwards to the next interface using a recursive formula.

- **The Limitation:** The recursive nature of this algorithm can be its Achilles' heel if not formulated correctly. The propagation terms involve exponentials of the form $e^{ik_z d}$, where d is the layer thickness and k_z is the vertical wavenumber. In highly conductive media like seawater, k_z has a large imaginary component, leading to extremely rapid decay (attenuation).

- **Numerical Instability:** When layers are electrically thick or highly lossy, these exponential terms can become vanishingly small (underflow) or astronomically large (overflow) during the recursion steps. This leads to numerical instability, where precision errors accumulate, often causing the solution to diverge.

Transfer Matrix Method (Propagator Matrix)

Another common technique is the Transfer Matrix Method (TMM). This method relates the electromagnetic fields at the top of a layer directly to the fields at the bottom via a 4×4 "propagator matrix." The global solution is found by multiplying the matrices of all individual layers together.

While conceptually straightforward, TMM suffers from the same numerical instability as recursive methods. The multiplication of matrices containing both exponentially growing and decaying terms ($e^{+ik_z d}$ and $e^{-ik_z d}$) results in a classic "loss of precision" problem. The growing terms (associated with evanescent waves) can overshadow the physical solution, making it difficult to extract the correct field coefficients, particularly in deep ocean models with many layers.

1.3.2 Full-Wave Numerical Methods

For more complex, arbitrary geometries (e.g., uneven seabed bathymetry or 3D targets), full-wave numerical methods are often employed.

Finite Element Method (FEM)

The Finite Element Method (FEM) is a powerful technique that discretizes the entire computational domain into a mesh of small elements (tetrahedra or hexahedra). It is considered the industry standard for modeling complex 3D geological structures where layers are not perfectly horizontal.

However, for large-scale stratified problems, FEM presents significant challenges:

- **Computational Cost:** To accurately model electromagnetic waves in conductive seawater, the mesh size must be a fraction of the skin depth. In a large-scale ocean environment (kilometers in range), this requires an enormous number of elements, leading to high memory usage and long computation times.
- **Boundary Truncation:** Unlike integral methods that naturally handle infinite domains, FEM requires artificial absorbing boundaries (like PML) to truncate the simulation space, which can introduce reflection artifacts if not placed sufficiently far from the source.

Finite Difference Time Domain (FDTD)

The Finite Difference Time Domain (FDTD) method solves Maxwell's equations directly in the time domain using a grid. While versatile, it suffers from dispersion errors and requires very long simulation times to reach a steady state for low-frequency diffusive EM problems common in underwater applications.

1.3.3 The Global Matrix Method (GMM)

Given the limitations of the methods described above—specifically the inability of homogeneous models to capture stratification and the numerical instability of Transfer Matrix methods in lossy media—there is a clear need for a more robust approach.

To address these challenges, this thesis employs the **Global Matrix Method (GMM)**. Unlike the Transfer Matrix Method, which propagates errors layer-by-layer through matrix multiplication, the Global Matrix Method formulates the boundary conditions at all interfaces simultaneously.

The distinct advantages of the GMM approach in the context of underwater electromagnetics include:

- **Numerical Stability:** The GMM formulation naturally suppresses the exponentially growing terms ($e^{+\gamma d}$) that cause overflow in standard propagator matrix methods. By organizing the field equations to track down-going waves in the upper layers and up-going waves in the lower layers, the system remains well-conditioned even for high-conductivity media like seawater.

- **Efficiency for Stratified Media**: While both methods ultimately assemble a global system of linear equations to find a solution, they approach the geometry differently. Finite Element Methods (FEM) require discretizing the entire spatial volume into meshes (which is computationally expensive for large offsets), whereas GMM solves the problem in the spectral domain by discretizing only the layer interfaces.

- **Rigorous Boundary Handling:** GMM explicitly enforces the continuity of tangential electric and magnetic fields across all N layers, capturing complex interference patterns and the lateral wave propagation that simpler models miss.

By utilizing the Global Matrix Method combined with a robust integration scheme (Romberg-Shanks), this thesis provides a stable and accurate tool for analyzing electromagnetic modes in realistic ocean environments.

1.4 Objectives of the Thesis

The primary objective of this research is to develop a robust theoretical and numerical framework for modeling electromagnetic wave propagation in a realistic, non-homogeneous seawater environment. By moving beyond the limitations of the homogeneous half-space model and the numerical instabilities of recursive algorithms, this thesis aims to provide a stable solution for N-layered media.

The specific objectives of this study are as follows:

1. **Theoretical Formulation:** To rigorously derive the electromagnetic field components (E_ρ, E_ϕ, E_z and H_ρ, H_ϕ, H_z) for a Horizontal Magnetic Dipole (HMD) submerged in a stratified medium. This involves utilizing the Hertz Vector Potential method and the Sommerfeld identity to convert the problem into the spectral domain.

2. **Implementation of the Global Matrix Method:** To formulate the boundary value problem using the Direct Global Matrix Method (DGMM). The goal is to construct a stable linear system that solves for the amplitude coefficients of all layers simultaneously, thereby eliminating the error accumulation inherent in recursive transmission line methods.

3. **Numerical Integration Algorithm:** To develop a custom numerical algorithm in Python to evaluate the highly oscillatory Sommerfeld integrals. This includes implementing the Romberg Integration method to achieve high precision in computing the inverse Hankel transforms required to convert spectral data back into the spatial domain.

4. **Simulation and Analysis:** To simulate the electromagnetic field distribution in various seawater profiles (e.g., presence of a thermocline). The study aims to investigate how vertical stratification affects the signal intensity and propagation characteristics compared to standard homogeneous models.

By achieving these objectives, this work seeks to provide a comprehensive tool for analyzing underwater electromagnetic propagation, with potential applications in designing more effective underwater communication systems and geophysical sensing arrays.

1.5 Thesis Outline

This thesis is organized into eight chapters, structured to guide the reader from fundamental physical principles to the advanced numerical implementation of the Global Matrix Method. The outline of the remaining chapters is as follows:

Chapter 2: Theoretical Formulation of the Electromagnetic Field derives the inhomogeneous vector Helmholtz equation from Maxwell's equations. It introduces the Hertz Vector Potential method, demonstrating how the coupled vector problem can be decomposed into independent scalar potentials (Π_e and Π_m) suitable for layered media analysis.

Chapter 3: Derivation of Field Components for a Horizontal Magnetic Dipole applies the Hertz potential formulation to the specific case of a Horizontal Magnetic Dipole (HMD). This chapter provides the rigorous derivation of the spectral integral representations for all six electromagnetic field components (E_ρ, E_ϕ, E_z and H_ρ, H_ϕ, H_z) in terms of Transverse Electric (TE) and Transverse Magnetic (TM) modes.

Chapter 4: The Direct Global Matrix Method details the core methodology of this research. It derives the electromagnetic boundary conditions at the interfaces of stratified media and constructs the "Global Matrix." This chapter explains how the boundary value problem is assembled into a single stable linear system, avoiding the numerical instabilities associated with recursive transmission line methods.

Chapter 5: Numerical Implementation and Solution describes the computational algorithm developed to solve the theoretical model. It details the discretization of the layers, the solution of the linear system, and the specific implementation of

the Romberg Integration method used to evaluate the highly oscillatory Sommerfeld integrals in Python.

Chapter 6: Results and Discussion presents the simulation results obtained from the numerical model. It validates the method against known analytical solutions and investigates the impact of non-homogeneous seawater profiles, such as the thermocline, on electromagnetic wave propagation.

Chapter 7: Conclusion and Future Work summarizes the key findings of the research, discusses the limitations of the current model, and offers recommendations for future studies to further enhance the accuracy and applicability of underwater electromagnetic modeling.

Chapter 2

Theoretical Formulation of the Electromagnetic Field

2.1 Physical Model of N-Layered Non-Homogeneous Seawater

To analyze the propagation of electromagnetic waves in a realistic marine environment, we must transition from the continuous variation of oceanographic parameters to a discrete mathematical model. As discussed in Chapter 1, the conductivity $\sigma(z)$ and permittivity $\epsilon(z)$ of seawater vary continuously with depth. To make the boundary value problem solvable, we approximate this continuous profile using an N-layered stratified model.

2.1.1 Geometric Configuration

We consider a cylindrical coordinate system (ρ, ϕ, z) where the z-axis is aligned vertically downwards. The environment is divided into N horizontal layers, indexed from $m = 1$ to $m = N$:

- **Layer 1 (Air):** The semi-infinite region above the sea surface ($z < z_1$), characterized by free-space parameters ($\epsilon_1, \mu_1, \sigma_1 \approx 0$).
- **Layers 2 to $N-1$ (Seawater):** A series of horizontal layers representing the water column. The m-th layer is bounded by interfaces at $z = z_{m-1}$ and $z = z_m$. The thickness of the m-th layer is $d_m = z_m - z_{m-1}$.
- **Layer N (Seabed):** The semi-infinite region below the water column ($z > z_{N-1}$), representing the sediment or crust.

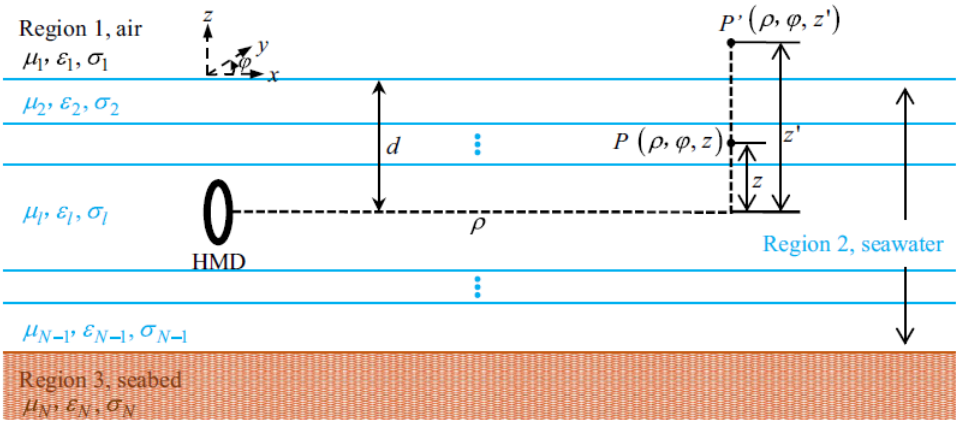

Figure 2.1: Geometry of the stratified conducting media model, illustrating the air, seawater, and seabed layers.[8].

2.1.2 Material Parameters

Within each layer m, the medium is assumed to be linear, isotropic, and homogeneous. The electromagnetic properties are defined by:

- **Conductivity (σ_m):** Represents the lossy nature of the medium (S/m).
- **Permittivity (ϵ_m):** Often expressed as the relative permittivity ϵ_r.
- **Permeability (μ_m):** Typically assumed to be equal to the free-space permeability μ_0 for non-magnetic seawater.

To account for the dissipative nature of the medium in the frequency domain, we define the **complex permittivity** $\hat{\epsilon}_m$ for the m-th layer as:

$$\hat{\epsilon}_m = \epsilon_m + i\frac{\sigma_m}{\omega} \tag{2.1}$$

where $\omega = 2\pi f$ is the angular frequency of the source. Consequently, the complex wavenumber k_m for each layer is given by:

$$k_m = \omega\sqrt{\mu_m\hat{\epsilon}_m} = \sqrt{\omega^2\mu_m\epsilon_m + i\omega\mu_m\sigma_m} \tag{2.2}$$

2.1.3 Source Configuration

A Horizontal Magnetic Dipole (HMD) is located at the coordinates $(0, 0, z_s)$ within the l-th layer (where $z_{l-1} < z_s < z_l$). The source is oriented along the x-axis with a

magnetic moment M_0. Mathematically, this source is represented as a current density distribution:

$$\mathbf{M}(\mathbf{r}) = M_0\delta(x)\delta(y)\delta(z - z_s)\hat{x} \tag{2.3}$$

This physical model forms the basis for the derivation of the wave equations in the subsequent sections.

2.2 Maxwell's Equations in Lossy Media

The propagation of electromagnetic waves is governed by Maxwell's equations. In a vacuum, waves propagate without loss. However, seawater is a dissipative (lossy) medium due to its high ionic conductivity. To model this, we must incorporate the conduction current density $\mathbf{J}$ into the fundamental equations.[16][17]

2.2.1 Time-Harmonic Representation

We assume that the electromagnetic fields oscillate harmonically with time. The instantaneous field $\mathcal{E}(\mathbf{r}, t)$ is related to the complex phasor $\mathbf{E}(\mathbf{r})$ by:

$$\mathcal{E}(\mathbf{r}, t) = \Re\{\mathbf{E}(\mathbf{r})e^{-i\omega t}\} \tag{2.4}$$

where $\omega = 2\pi f$ is the angular frequency and $i = \sqrt{-1}$. Consequently, the time derivative operator is replaced by multiplication by $-i\omega$:

$$\frac{\partial}{\partial t} \to -i\omega \tag{2.5}$$

2.2.2 Frequency Domain Equations

For a linear, isotropic, and homogeneous region within the seawater, Maxwell's equations in differential form are:

$$\nabla \times \mathbf{E} = i\omega\mathbf{B} - \mathbf{M} \tag{2.6}$$

$$\nabla \times \mathbf{H} = -i\omega\mathbf{D} + \mathbf{J} \tag{2.7}$$

$$\nabla \cdot \mathbf{D} = \rho_e \tag{2.8}$$

$$\nabla \cdot \mathbf{B} = \rho_m \tag{2.9}$$

Here, we have included a magnetic current density $\mathbf{M}$ to represent the source (the magnetic dipole), while $\mathbf{J}$ represents the electric current density flowing in the medium.

2.2.3 Constitutive Relations and Complex Permittivity

To solve these equations, we apply the constitutive relations for seawater:

$$\mathbf{D} = \epsilon \mathbf{E} \tag{2.10}$$

$$\mathbf{B} = \mu \mathbf{H} \tag{2.11}$$

$$\mathbf{J} = \sigma \mathbf{E} \quad \text{(Ohm's Law)} \tag{2.12}$$

Substituting these into Ampere's Law (2.7):

$$\nabla \times \mathbf{H} = -i\omega\epsilon \mathbf{E} + \sigma \mathbf{E} = -i\omega \left(\epsilon + i\frac{\sigma}{\omega}\right) \mathbf{E} \tag{2.13}$$

The term in the parentheses is defined as the complex permittivity $\hat{\epsilon}$:

$$\hat{\epsilon} = \epsilon + i\frac{\sigma}{\omega} = \epsilon_0 \epsilon_r + i\frac{\sigma}{\omega} \tag{2.14}$$

This single parameter captures both the displacement current (dielectric effect) and the conduction current (ohmic loss). Similarly, we define the squared complex wavenumber k^2 as:

$$k^2 = \omega^2 \mu \hat{\epsilon} = \omega^2 \mu \epsilon + i\omega\mu\sigma \tag{2.15}$$

In the low-frequency limit (ELF/VLF) relevant to underwater communication, $\sigma \gg \omega\epsilon$, meaning conduction currents dominate displacement currents ($k^2 \approx i\omega\mu\sigma$).

2.2.4 Final System of Equations

With these definitions, the coupled first-order Maxwell's equations simplify to a symmetric form ideal for derivation:

$$\nabla \times \mathbf{E} = i\omega\mu \mathbf{H} - \mathbf{M} \tag{2.16}$$

$$\nabla \times \mathbf{H} = -i\omega\hat{\epsilon} \mathbf{E} \tag{2.17}$$

These two equations form the starting point for deriving the vector Helmholtz equation in the next section.

2.3 Derivation of the Vector Helmholtz Equation

In the previous section, we established Maxwell's equations as a system of coupled first-order differential equations. While physically complete, this coupled form is difficult to solve directly because the Electric field ($\mathbf{E}$) depends on the Magnetic field ($\mathbf{H}$), and vice versa. To facilitate a solution, we must decouple these fields to obtain a

single equation governing the behavior of each vector field independently. This second-order partial differential equation is known as the Vector Helmholtz Equation.[13]

2.3.1 Decoupling the Fields

We begin with the frequency-domain Faraday's Law derived in Eq. (2.6):

$$\nabla \times \mathbf{E} = i\omega\mu\mathbf{H} - \mathbf{M} \tag{2.18}$$

To eliminate $\mathbf{H}$ from this equation, we take the curl ($\nabla\times$) of both sides:

$$\nabla \times (\nabla \times \mathbf{E}) = i\omega\mu(\nabla \times \mathbf{H}) - \nabla \times \mathbf{M} \tag{2.19}$$

Now, we substitute Ampere's Law ($\nabla \times \mathbf{H} = -i\omega\hat{\epsilon}\mathbf{E}$) into the right-hand side. Note that we assume the medium within the layer is homogeneous, meaning μ and $\hat{\epsilon}$ are spatially constant scalars and can be pulled out of the derivative operators.

$$\nabla \times (\nabla \times \mathbf{E}) = i\omega\mu(-i\omega\hat{\epsilon}\mathbf{E}) - \nabla \times \mathbf{M} \tag{2.20}$$

Simplifying the scalar coefficients:

$$\nabla \times (\nabla \times \mathbf{E}) = \omega^2\mu\hat{\epsilon}\mathbf{E} - \nabla \times \mathbf{M} \tag{2.21}$$

Recalling the definition of the complex wavenumber $k^2 = \omega^2\mu\hat{\epsilon}$, this becomes:

$$\nabla \times (\nabla \times \mathbf{E}) = k^2\mathbf{E} - \nabla \times \mathbf{M} \tag{2.22}$$

2.3.2 Applying Vector Identities

The left-hand side of Eq. (2.22) is a "curl of a curl." We apply the standard vector identity(appendix A):

$$\nabla \times (\nabla \times \mathbf{E}) = \nabla(\nabla \cdot \mathbf{E}) - \nabla^2\mathbf{E} \tag{2.23}$$

In a region with no free electric charge ($\rho_e = 0$), Gauss's Law states that $\nabla \cdot \mathbf{E} = 0$. Therefore, the gradient term vanishes ($\nabla(\nabla \cdot \mathbf{E}) = 0$), and the identity simplifies to:

$$\nabla \times (\nabla \times \mathbf{E}) = -\nabla^2\mathbf{E} \tag{2.24}$$

Substituting this back into Eq. (2.22):

$$-\nabla^2\mathbf{E} = k^2\mathbf{E} - \nabla \times \mathbf{M} \tag{2.25}$$

2.3.3 The Inhomogeneous Wave Equation

Rearranging the terms to group the field components on the left and the source term on the right, we arrive at the **Inhomogeneous Vector Helmholtz Equation** for the electric field:

$$\nabla^2\mathbf{E} + k^2\mathbf{E} = \nabla \times \mathbf{M} \tag{2.26}$$

This equation states that the Laplacian of the electric field, plus a term proportional to the field itself, is driven by the curl of the magnetic source distribution.

By following a similar procedure—taking the curl of Ampere's Law and substituting Faraday's Law—we can derive the corresponding equation for the magnetic field:

$$\nabla^2\mathbf{H} + k^2\mathbf{H} = -i\omega\hat{\epsilon}\mathbf{M} - \nabla \times \left(\frac{\mathbf{M}}{\mu}\right) \times \mu \ldots \tag{2.27}$$

However, solving these vector equations directly for $\mathbf{E}$ and $\mathbf{H}$ in cylindrical coordinates is mathematically cumbersome because the unit vectors $(\hat{\rho}, \hat{\phi})$ themselves depend on position. To avoid this complexity, we will instead solve for auxiliary scalar potentials (Hertz Potentials) in the following section, which allow us to treat the problem using scalar wave equations.

2.4 Hertz Vector Potentials

Directly solving the vector Helmholtz equation derived in Section 2.3 is mathematically arduous because the electric and magnetic field components are coupled. To simplify the problem, we introduce auxiliary potential functions known as Hertz vectors. These potentials allow us to reduce the coupled vector problem into independent scalar wave equations, which are amenable to solution in cylindrical coordinates.

We define two types of Hertz vectors corresponding to the two possible source types:

1. **Electric Hertz Vector ($\mathbf{\Pi}_e$):** Used for electric current sources ($\mathbf{J}$) and generates Transverse Magnetic (TM) modes.

2. **Magnetic Hertz Vector ($\mathbf{\Pi}_m$):** Used for magnetic current sources ($\mathbf{M}$) and generates Transverse Electric (TE) modes.

2.4.1 Electric Hertz Vector ($\mathbf{\Pi}_e$)

Consider a region with an electric current source $\mathbf{J}$ but no magnetic source ($\mathbf{M} = 0$). Maxwell's equations imply that the magnetic flux density is solenoidal:

$$\nabla \cdot \mathbf{B} = \nabla \cdot (\mu\mathbf{H}) = 0 \implies \nabla \cdot \mathbf{H} = 0 \tag{2.28}$$

Since the divergence of $\mathbf{H}$ is zero, it can be expressed as the curl of a vector potential. We define the **Electric Hertz Vector** $\mathbf{\Pi}_e$ such that the magnetic field is given by:

$$\boxed{\mathbf{H} = -i\omega\hat{\epsilon}\nabla \times \mathbf{\Pi}_e} \tag{2.29}$$

Substituting this into Ampere's Law ($\nabla \times \mathbf{H} = -i\omega\hat{\epsilon}\mathbf{E} + \mathbf{J}$ is not suitable here; we use the source-free form $\nabla \times \mathbf{H} = -i\omega\hat{\epsilon}\mathbf{E}$ to find the relation, then add the source to the wave equation). Rearranging for $\mathbf{E}$:

$$\mathbf{E} = \frac{1}{-i\omega\hat{\epsilon}}(\nabla \times \mathbf{H}) = \frac{1}{-i\omega\hat{\epsilon}}\nabla \times (-i\omega\hat{\epsilon}\nabla \times \mathbf{\Pi}_e) = \nabla \times \nabla \times \mathbf{\Pi}_e \tag{2.30}$$

Using the vector identity $\nabla \times \nabla \times \mathbf{A} = \nabla(\nabla \cdot \mathbf{A}) - \nabla^2\mathbf{A}$, we obtain:

$$\boxed{\mathbf{E} = \nabla(\nabla \cdot \mathbf{\Pi}_e) + k^2\mathbf{\Pi}_e} \tag{2.31}$$

Substituting these fields into the wave equation, it can be shown that $\mathbf{\Pi}_e$ satisfies the inhomogeneous Helmholtz equation driven by the electric source $\mathbf{J}$:

$$\nabla^2\mathbf{\Pi}_e + k^2\mathbf{\Pi}_e = -\frac{\mathbf{J}}{-i\omega\hat{\epsilon}} \tag{2.32}$$

2.4.2 Magnetic Hertz Vector ($\mathbf{\Pi}_m$)

Now consider the case relevant to our Horizontal Magnetic Dipole, where we have a magnetic source $\mathbf{M}$ (and $\mathbf{J} = 0$). Maxwell's equations imply that the electric flux density is solenoidal:

$$\nabla \cdot \mathbf{D} = \nabla \cdot (\hat{\epsilon}\mathbf{E}) = 0 \implies \nabla \cdot \mathbf{E} = 0 \tag{2.33}$$

We define the **Magnetic Hertz Vector** $\mathbf{\Pi}_m$ such that the electric field is given by the curl of the potential:

$$\boxed{\mathbf{E} = -i\omega\mu\nabla \times \mathbf{\Pi}_m} \tag{2.34}$$

Substituting this into Faraday's Law ($\nabla \times \mathbf{E} = i\omega\mu\mathbf{H}$), we solve for $\mathbf{H}$.

$$i\omega\mu\mathbf{H} = \nabla \times \mathbf{E} = \nabla \times (-i\omega\mu\nabla \times \mathbf{\Pi}_m) \tag{2.35}$$

Canceling the $i\omega\mu$ terms (and applying the Gauge condition $\Phi_m = \nabla \cdot \mathbf{\Pi}_m$ as discussed in standard texts), we arrive at:

$$\boxed{\mathbf{H} = \nabla(\nabla \cdot \mathbf{\Pi}_m) + k^2\mathbf{\Pi}_m = \nabla \times \nabla \times \mathbf{\Pi}_m} \tag{2.36}$$

Substituting these into the wave equation, $\mathbf{\Pi}_m$ satisfies:

$$\nabla^2 \mathbf{\Pi}_m + k^2 \mathbf{\Pi}_m = -\frac{\mathbf{M}}{i\omega\mu} \tag{2.37}$$

2.4.3 General Solution for Layered Media

In a general stratified medium, the electromagnetic field is a superposition of TE and TM modes. To represent an arbitrary field, we use a combination of both potentials aligned with the vertical z-axis:

$$\mathbf{\Pi} = \Pi_e \hat{z} + \Pi_m \hat{z} \tag{2.38}$$

- $\Pi_e \hat{z}$ generates the **TM mode** ($H_z = 0$).
- $\Pi_m \hat{z}$ generates the **TE mode** ($E_z = 0$).

This decomposition is crucial for Chapter 3, where we will solve for the field components of the Horizontal Magnetic Dipole.

2.5 General Solution in Cylindrical Coordinates

Having reduced the vector electromagnetic problem to a set of scalar Helmholtz equations for the Hertz potentials (Π), we now seek a general solution in the cylindrical coordinate system (ρ, ϕ, z). This coordinate system is chosen to match the planar symmetry of the stratified ocean environment.

The homogeneous scalar Helmholtz equation is given by:

$$\nabla^2 \psi(\mathbf{r}) + k^2 \psi(\mathbf{r}) = 0 \tag{2.39}$$

where ψ represents any Cartesian component of the Hertz vectors (e.g., Π_{mz}).

2.5.1 Separation of Variables

In cylindrical coordinates, the Laplacian operator is:

$$\nabla^2 = \frac{1}{\rho}\frac{\partial}{\partial \rho}\left(\rho \frac{\partial}{\partial \rho}\right) + \frac{1}{\rho^2}\frac{\partial^2}{\partial \phi^2} + \frac{\partial^2}{\partial z^2} \tag{2.40}$$

We assume a separable solution of the form:

$$\psi(\rho, \phi, z) = R(\rho)\Phi(\phi)Z(z) \tag{2.41}$$

Substituting this into Eq. (2.39) and dividing by ψ, we obtain:

$$\frac{1}{R}\left[\frac{1}{\rho}\frac{d}{d\rho}\left(\rho\frac{dR}{d\rho}\right)\right] + \frac{1}{\rho^2\Phi}\frac{d^2\Phi}{d\phi^2} + \frac{1}{Z}\frac{d^2Z}{dz^2} + k^2 = 0 \tag{2.42}$$

To separate the variables, we introduce a separation constant k_ρ^2 (the radial wavenumber) and k_z (the vertical wavenumber).

1. Vertical Dependence (z): Isolating the z-term, we set:

$$\frac{1}{Z}\frac{d^2Z}{dz^2} = -k_z^2 \implies \frac{d^2Z}{dz^2} + k_z^2 Z = 0 \tag{2.43}$$

The solution to this harmonic equation describes wave propagation in the vertical direction:

$$Z(z) = Ae^{ik_z z} + Be^{-ik_z z} \tag{2.44}$$

Here, k_z is related to the radial wavenumber by the dispersion relation: $k_z^2 = k^2 - k_\rho^2$.

2. Azimuthal Dependence (ϕ): Isolating the ϕ-term, we set the separation constant to $-n^2$ (where n is an integer for physical uniqueness):

$$\frac{1}{\Phi}\frac{d^2\Phi}{d\phi^2} = -n^2 \implies \frac{d^2\Phi}{d\phi^2} + n^2\Phi = 0 \tag{2.45}$$

The solutions are harmonic functions: $\sin(n\phi)$ and $\cos(n\phi)$.

3. Radial Dependence (ρ): The remaining radial equation becomes:

$$\rho^2\frac{d^2R}{d\rho^2} + \rho\frac{dR}{d\rho} + (k_\rho^2\rho^2 - n^2)R = 0 \tag{2.46}$$

This is the standard **Bessel Differential Equation** of order n.

2.5.2 Bessel Functions and Hankel Transforms

The general solution to the Bessel equation (Eq. 2.46) is a linear combination of Bessel functions of the first kind $J_n(k_\rho\rho)$ and second kind $Y_n(k_\rho\rho)$. However, for wave propagation problems involving radiation to infinity, it is physically more convenient to use **Hankel functions**:

$$H_n^{(1)}(x) = J_n(x) + iY_n(x) \quad \text{(Incoming wave)} \tag{2.47}$$

$$H_n^{(2)}(x) = J_n(x) - iY_n(x) \quad \text{(Outgoing wave)} \tag{2.48}$$

Assuming a time dependence of $e^{-i\omega t}$, the Hankel function of the first kind $H_n^{(1)}(k_\rho\rho)$ represents a converging wave, while $H_n^{(2)}$ is usually discarded or used carefully depending on the sign convention. (With the $e^{-i\omega t}$ convention used, $H_n^{(1)}$ typically

corresponds to outgoing waves).

The Sommerfeld Integral Representation

Since the separation parameter k_ρ can take any continuous value from 0 to ∞, the general solution is constructed by integrating over all possible radial wavenumbers. This superposition is known as the **Sommerfeld Integral** or the inverse **Hankel Transform**:

$$\psi(\rho, \phi, z) = \sum_{n=0}^{\infty} \cos(n\phi) \int_0^{\infty} \tilde{Z}(k_\rho, z, k_z) J_n(k_\rho \rho) k_\rho \, dk_\rho \tag{2.49}$$

This integral transforms the problem from the spatial domain (ρ, z) to the spectral domain (k_ρ, z). In the spectral domain, the partial differential equations reduce to ordinary differential equations in z, which are far easier to solve for layered media.

This formulation is the foundation for the "Global Matrix Method," where we solve for the spectral amplitudes $\tilde{Z}$ in every layer before numerically integrating back to the spatial domain.

Chapter 3

Field Components for a Horizontal Magnetic Dipole (HMD)

3.1 Primary Field of the Magnetic Dipole

The total electromagnetic field in a stratified medium is composed of two parts: the **primary field**, which represents the direct radiation from the source in an unbounded medium, and the **secondary field**, which accounts for the reflections and refractions from the layer interfaces.The radiation characteristics of a dipole submerged in a lossy medium differ significantly from the free-space case, as detailed by King and Smith [5]. In this section, we derive the expression for the primary field.

3.1.1 Source Definition

We consider a Horizontal Magnetic Dipole (HMD) located at the origin of the coordinate system $(0, 0, z_s)$. Without loss of generality, we align the dipole moment along the x-axis. The magnetic current density $\mathbf{M}$ is mathematically represented using the Dirac delta function:

$$\mathbf{M}(\mathbf{r}) = M_0\delta(x)\delta(y)\delta(z - z_s)\hat{x} \tag{3.1}$$

where $M_0 = IA$ is the magnetic moment (current I times loop area A) [12].

3.1.2 Primary Hertz Vector Potential

From Chapter 2, we know that the Magnetic Hertz Vector $\mathbf{\Pi}_m$ satisfies the inhomogeneous Helmholtz equation:

$$\nabla^2\mathbf{\Pi}_m + k^2\mathbf{\Pi}_m = -\frac{\mathbf{M}}{i\omega\mu} \tag{3.2}$$

Substituting the source term:

$$\nabla^2 \mathbf{\Pi}_m + k^2 \mathbf{\Pi}_m = -\frac{M_0}{i\omega\mu}\delta(\mathbf{r} - \mathbf{r}_s)\hat{x} \tag{3.3}$$

Since the source is oriented entirely in the $\hat{x}$ direction, the primary Hertz potential will also be oriented in the $\hat{x}$ direction. The scalar part of this equation is identical to the Green's function equation derived in Appendix A. Therefore, the solution is simply the free-space Green's function scaled by the source magnitude:

$$\mathbf{\Pi}_m^{prim} = \frac{M_0}{i\omega\mu}G(R)\hat{x} = \frac{M_0}{4\pi i\omega\mu}\frac{e^{ikR}}{R}\hat{x} \tag{3.4}$$

where $R = \sqrt{\rho^2 + (z - z_s)^2}$ is the distance from the source. For brevity, we define the source strength constant $C_{HM} = \frac{M_0}{4\pi i\omega\mu}$.

3.1.3 Coordinate Transformation

While the source is Cartesian (x-directed), our boundary value problem is Cylindrical. We must transform the unit vector $\hat{x}$ into cylindrical coordinates $(\hat{\rho}, \hat{\phi}, \hat{z})$ using the transformation derived in Appendix A:

$$\hat{x} = \cos\phi\,\hat{\rho} - \sin\phi\,\hat{\phi} \tag{3.5}$$

Substituting this into the potential expression:

$$\mathbf{\Pi}_m^{prim} = C_{HM}\frac{e^{ikR}}{R}(\cos\phi\,\hat{\rho} - \sin\phi\,\hat{\phi}) \tag{3.6}$$

This equation reveals a critical difficulty: the primary field has components in both the radial ($\hat{\rho}$) and azimuthal ($\hat{\phi}$) directions, and these components depend on the angle ϕ. This angular dependence ($\cos\phi$ and $\sin\phi$) means the problem is not azimuthally symmetric.

To satisfy the planar boundary conditions at $z = z_m$ in the subsequent sections, we cannot simply use this spherical wave form (e^{ikR}/R). We must expand this spherical wave into a spectrum of cylindrical waves, a process achieved using the **Sommerfeld Identity**.

3.2 Sommerfeld Identity and Spectral Expansion

The primary field expression derived in Section 3.1 describes a spherical wave radiating from a point source. However, the stratified ocean environment is defined by

planar interfaces (z = constant). To satisfy the boundary conditions at these interfaces, we must transform the spherical wave into a superposition of plane waves (spectral representation). This transformation is rigorously achieved by deriving the **Sommerfeld Identity** starting from the 3D Fourier domain. While methods such as Complex Image Theory [6] provide approximations, we employ the rigorous spectral expansion method.

3.2.1 The Weyl Identity (Cartesian Spectral Domain)

We begin by defining the scalar Green's function $G(\mathbf{r})$ using a 3D Fourier Transform. The relationship between the spatial domain $G(\mathbf{r})$ and the spectral domain $\tilde{G}(\mathbf{k})$ is given by[17]:

$$G(\mathbf{r}) = \frac{1}{(2\pi)^3} \iiint_{-\infty}^{\infty} \tilde{G}(\mathbf{k}) e^{i\mathbf{k}\cdot\mathbf{r}}\, d^3k \tag{3.7}$$

where $\mathbf{k} = k_x\hat{x} + k_y\hat{y} + k_z\hat{z}$ is the wave vector. Substituting this into the inhomogeneous Helmholtz equation $(\nabla^2 + k_0^2)G(\mathbf{r}) = -\delta(\mathbf{r})$, the differential operator ∇^2 becomes $-k^2$ in the spectral domain [1].

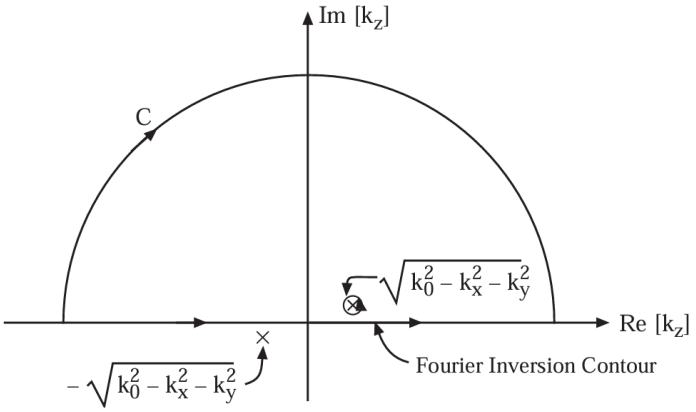

Figure 3.1: The integration along the real axis is equal to the integration along the contour C plus the residue of the pole at $(k_0^2 - k_x^2 - k_y^2)^{1/2}$, by invoking Jordan's lemma.[18].

This yields the algebraic solution:

$$\tilde{G}(\mathbf{k}) = \frac{1}{k^2 - k_0^2} = \frac{1}{k_x^2 + k_y^2 + k_z^2 - k_0^2} \tag{3.8}$$

The spatial domain Green's function is retrieved by the inverse transform:

$$G(\mathbf{r}) = \frac{1}{(2\pi)^3} \iint_{-\infty}^{\infty} dk_x dk_y\, e^{i(k_x x + k_y y)} \left[\int_{-\infty}^{\infty} \frac{e^{ik_z z}}{k_z^2 - (k_0^2 - k_x^2 - k_y^2)}\, dk_z \right] \tag{3.9}$$

Evaluation via Cauchy's Residue Theorem

To evaluate the inner integral over k_z, we define the vertical spectral wavenumber k_{z0} such that $k_{z0}^2 = k_0^2 - k_x^2 - k_y^2$. The integrand has simple poles at $k_z = \pm k_{z0}$.

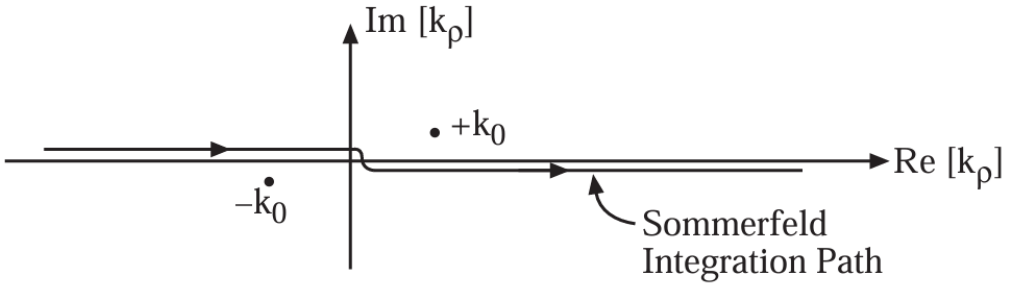

Figure 3.2: The Sommerfeld integration path (SIP) in the complex λ-plane. The contour is deformed to avoid the branch point singularity at k_0 and the surface wave poles. [18].

We apply **Cauchy's Residue Theorem**. For $z > 0$, we must close the contour in the upper half of the complex k_z-plane ($\mathrm{Im}(k_z) > 0$) to satisfy Jordan's Lemma, ensuring the contribution from the infinite arc vanishes. The pole at $+k_{z0}$ lies inside this contour [1].

The residue at $k_z = k_{z0}$ is calculated as:

$$\text{Residue} = \lim_{k_z \to k_{z0}} (k_z - k_{z0}) \frac{e^{ik_z z}}{(k_z - k_{z0})(k_z + k_{z0})} \tag{3.10}$$

$$= \frac{e^{ik_{z0} z}}{2k_{z0}} \tag{3.11}$$

By the Residue Theorem, the value of the integral is $2\pi i \times$ Residue. Substituting this back into Eq. (3.9) yields the **Weyl Identity** [19]:

$$\frac{e^{ik_0 r}}{r} = \frac{i}{2\pi} \iint_{-\infty}^{\infty} \frac{e^{i(k_x x + k_y y + k_{z0}|z|)}}{k_{z0}} \, dk_x \, dk_y \tag{3.12}$$

This equation expresses the spherical wave as a superposition of plane waves propagating in all Cartesian directions.

3.2.2 Transformation to Cylindrical Coordinates

To match the cylindrical symmetry, we transform the spectral variables (k_x, k_y) to cylindrical spectral coordinates (k_ρ, α) [7]:

$$k_x = k_\rho \cos\alpha, \quad k_y = k_\rho \sin\alpha \tag{3.13}$$

The differential area element transforms using the Jacobian(Appendix A):

$$dk_x dk_y = k_\rho \, dk_\rho \, d\alpha \tag{3.14}$$

Similarly, the spatial coordinates are transformed as $x = \rho\cos\phi, y = \rho\sin\phi$. The phase term in the exponential becomes:

$$k_x x + k_y y = k_\rho \rho(\cos\alpha\cos\phi + \sin\alpha\sin\phi) = k_\rho \rho\cos(\alpha - \phi) \tag{3.15}$$

Substituting these into the Weyl Identity allows us to separate the angular and radial integrals:

$$\frac{e^{ik_0 r}}{r} = \frac{i}{2\pi}\int_0^\infty \frac{k_\rho}{k_{z0}} e^{ik_{z0}|z|}\left[\int_0^{2\pi} e^{ik_\rho \rho\cos(\alpha-\phi)}\, d\alpha\right] dk_\rho \tag{3.16}$$

3.2.3 The Sommerfeld Integral Identity

The inner integral over α corresponds to the integral representation of the Bessel function of the first kind, order zero, $J_0(k_\rho\rho)$[20][10]:

$$J_0(x) = \frac{1}{2\pi}\int_0^{2\pi} e^{ix\cos\beta}\, d\beta \tag{3.17}$$

Using this definition, we arrive at the renowned Sommerfeld Identity[7]:

$$\boxed{\frac{e^{ik_0 r}}{r} = i\int_0^\infty \frac{k_\rho}{k_{z0}} J_0(k_\rho\rho) e^{ik_{z0}|z|}\, dk_\rho} \tag{3.18}$$

where $k_{z0} = \sqrt{k_0^2 - k_\rho^2}$. This identity is the fundamental tool that allows us to treat the spherical radiation from the dipole as a bundle of cylindrical waves.

3.2.4 Extension to Hankel Functions

For numerical evaluation, it is advantageous to extend the range of integration to $(-\infty, \infty)$ using Hankel functions. We use the identity $J_0(x) = \frac{1}{2}[H_0^{(1)}(x) + H_0^{(2)}(x)]$ [16]. Through the symmetry property $H_0^{(2)}(x) = -H_0^{(1)}(-x)$, we can fold the integration range [8]. This leads to the form used in the Global Matrix Method:

$$\frac{e^{ik_0 r}}{r} = \frac{i}{2}\int_{-\infty}^\infty \frac{k_\rho}{k_{z0}} H_0^{(1)}(k_\rho\rho) e^{ik_{z0}|z|}\, dk_\rho \tag{3.19}$$

This representation is particularly robust for leaky mode analysis as it deals with traveling waves rather than standing waves.

3.3 Spectral Representation of Field Components

Having established the spectral expansion of the scalar potential in Section 3.2, we now derive the expressions for the six electromagnetic field components (E_ρ, E_ϕ, E_z and H_ρ, H_ϕ, H_z) in the cylindrical coordinate system.

To analyze the field in a stratified medium, it is convenient to decompose the total electromagnetic field into two independent modes relative to the vertical direction (z):

1. **Transverse Magnetic (TM) Mode:** Characterized by $H_z = 0$. This mode is generated purely by the Electric Hertz vector $\mathbf{\Pi}_e = \psi_e \hat{z}$.
2. **Transverse Electric (TE) Mode:** Characterized by $E_z = 0$. This mode is generated purely by the Magnetic Hertz vector $\mathbf{\Pi}_m = \psi_m \hat{z}$.

The total field produced by the Horizontal Magnetic Dipole is a superposition of these two modes.

3.3.1 Transverse Magnetic (TM) Field Components

The TM field components are derived from the vertical Electric Hertz potential ψ_e. From the Maxwell-Hertz relations derived in Eq. (2.34) and Eq. (2.36):

$$\mathbf{H}^{TM} = -i\omega\hat{\epsilon}\nabla \times (\psi_e \hat{z}) \tag{3.20}$$

$$\mathbf{E}^{TM} = \nabla \times \nabla \times (\psi_e \hat{z}) \tag{3.21}$$

Magnetic Field (H^{TM})

Computing the curl in cylindrical coordinates:

$$\nabla \times (\psi_e \hat{z}) = \left(\frac{1}{\rho} \frac{\partial \psi_e}{\partial \phi} \hat{\rho} - \frac{\partial \psi_e}{\partial \rho} \hat{\phi} \right) \tag{3.22}$$

Multiplying by $-i\omega\hat{\epsilon}$, we obtain the magnetic components:

$$H_\rho^{TM} = -i\omega\hat{\epsilon} \frac{1}{\rho} \frac{\partial \psi_e}{\partial \phi} \tag{3.23}$$

$$H_\phi^{TM} = i\omega\hat{\epsilon} \frac{\partial \psi_e}{\partial \rho} \tag{3.24}$$

$$H_z^{TM} = 0 \tag{3.25}$$

Electric Field (E^{TM})

Using the identity $\nabla \times \nabla \times \mathbf{A} = \nabla(\nabla \cdot \mathbf{A}) - \nabla^2 \mathbf{A}$ and noting that $\nabla^2(\psi_e \hat{z}) = -k^2 \psi_e \hat{z}$ (from the Helmholtz equation):

$$\mathbf{E}^{TM} = \nabla \left(\frac{\partial \psi_e}{\partial z} \right) + k^2 \psi_e \hat{z} \tag{3.26}$$

Computing the gradient components:

$$E_\rho^{TM} = \frac{\partial^2 \psi_e}{\partial \rho \partial z} \tag{3.27}$$

$$E_\phi^{TM} = \frac{1}{\rho} \frac{\partial^2 \psi_e}{\partial \phi \partial z} \tag{3.28}$$

$$E_z^{TM} = \frac{\partial^2 \psi_e}{\partial z^2} + k^2 \psi_e \tag{3.29}$$

3.3.2 Transverse Electric (TE) Field Components

The TE field components are derived from the vertical Magnetic Hertz potential ψ_m.:

$$\mathbf{E}^{TE} = i\omega\mu \nabla \times (\psi_m \hat{z}) \tag{3.30}$$

$$\mathbf{H}^{TE} = \nabla \times \nabla \times (\psi_m \hat{z}) \tag{3.31}$$

Electric Field (E^{TE})

Similarly to the magnetic case above, calculating the curl yields:

$$E_\rho^{TE} = i\omega\mu \frac{1}{\rho} \frac{\partial \psi_m}{\partial \phi} \tag{3.32}$$

$$E_\phi^{TE} = -i\omega\mu \frac{\partial \psi_m}{\partial \rho} \tag{3.33}$$

$$E_z^{TE} = 0 \tag{3.34}$$

Magnetic Field (H^{TE})

Applying the curl-curl operation yields:

$$H_\rho^{TE} = \frac{\partial^2 \psi_m}{\partial \rho \partial z} \tag{3.35}$$

$$H_\phi^{TE} = \frac{1}{\rho} \frac{\partial^2 \psi_m}{\partial \phi \partial z} \tag{3.36}$$

$$H_z^{TE} = \frac{\partial^2 \psi_m}{\partial z^2} + k^2 \psi_m \tag{3.37}$$

3.3.3 Total Field Expressions

The total electromagnetic field is the vector sum of the TE and TM contributions. In the spectral domain, we replace the potentials with their integral representations involving Bessel functions. Let the potentials be expressed as Sommerfeld integrals:

$$\psi_{e,m}(\rho, \phi, z) = \mathcal{F}_{e,m}(\phi) \int_0^\infty \tilde{\psi}_{e,m}(k_\rho, z) J_n(k_\rho \rho) k_\rho \, dk_\rho \tag{3.38}$$

Substituting these into the component equations derived above, the spatial derivatives transform as follows:

- $\frac{\partial}{\partial z} \to ik_z$ (for upward traveling waves)
- $\frac{\partial}{\partial \rho} J_n(k_\rho \rho) \to k_\rho J_n'(k_\rho \rho)$

The complete set of field components in the cylindrical spectral domain is:

$$E_\rho = \frac{\partial^2 \psi_e}{\partial \rho \partial z} + \frac{i\omega\mu}{\rho} \frac{\partial \psi_m}{\partial \phi} \tag{3.39}$$

$$E_\phi = \frac{1}{\rho} \frac{\partial^2 \psi_e}{\partial \phi \partial z} - i\omega\mu \frac{\partial \psi_m}{\partial \rho} \tag{3.40}$$

$$E_z = \left(k^2 + \frac{\partial^2}{\partial z^2} \right) \psi_e \tag{3.41}$$

$$H_\rho = \frac{\partial^2 \psi_m}{\partial \rho \partial z} - \frac{i\omega\hat{\epsilon}}{\rho} \frac{\partial \psi_e}{\partial \phi} \tag{3.42}$$

$$H_\phi = \frac{1}{\rho} \frac{\partial^2 \psi_m}{\partial \phi \partial z} + i\omega\hat{\epsilon} \frac{\partial \psi_e}{\partial \rho} \tag{3.43}$$

$$H_z = \left(k^2 + \frac{\partial^2}{\partial z^2} \right) \psi_m \tag{3.44}$$

These six equations form the basis for the Global Matrix Method. In Chapter 3, we will equate the tangential components $(E_\rho, E_\phi, H_\rho, H_\phi)$ across layer interfaces to solve for the unknown potential amplitudes.

3.4 Electric Field Components (E_ρ, E_ϕ, E_z)

In this section, we rigorously derive the explicit spectral integral expressions for the electric field components. We begin with the scalar potentials for the HMD, which incorporate the specific angular dependence of the source.

3.4.1 Potentials and Operators

The azimuthal dependencies of the Hertz potentials—specifically $\sin\phi$ for the electric potential (ψ_e) and $\cos\phi$ for the magnetic potential (ψ_m)—originate from the coordinate transformation of the primary source. For a horizontal magnetic dipole (HMD) oriented along the x-axis, the primary source unit vector $\hat{x}$ is projected into cylindrical coordinates as:

$$\hat{x} = \cos\phi\hat{\rho} - \sin\phi\hat{\phi} \tag{3.45}$$

This geometric projection splits the electromagnetic field into distinct radial and azimuthal components. Consequently, the magnetic Hertz potential (ψ_m), which generates the Transverse Electric (TE) mode and aligns with the radial outward projection of the source, adopts the $\cos\phi$ dependence. Conversely, the electric Hertz potential (ψ_e), which generates the Transverse Magnetic (TM) mode representing the induced orthogonal fields, inherently follows the azimuthal $\sin\phi$ projection. Therefore, we express the general forms of the potentials as:

$$\psi_m = \Psi_m(\rho, z)\cos\phi \tag{3.46}$$

$$\psi_e = \Psi_e(\rho, z)\sin\phi \tag{3.47}$$

The spectral definitions of the Hertz potentials in layer j:

$$\psi_e(\rho, \phi, z) = \sin\phi \int_0^\infty \tilde{\psi}_e(z, k_\rho) J_1(k_\rho\rho) k_\rho \, dk_\rho \tag{3.48}$$

$$\psi_m(\rho, \phi, z) = \cos\phi \int_0^\infty \tilde{\psi}_m(z, k_\rho) J_1(k_\rho\rho) k_\rho \, dk_\rho \tag{3.49}$$

where $\tilde{\psi}_e$ and $\tilde{\psi}_m$ contain the vertical propagation terms (e.g., $A_j e^{-ik_{zj}z} + \dots$).

The general operators for the electric field components (derived in Section 3.3) are:

$$E_\rho = \frac{\partial^2\psi_e}{\partial\rho\partial z} - \frac{i\omega\mu}{\rho}\frac{\partial\psi_m}{\partial\phi} \tag{3.50}$$

$$E_\phi = \frac{1}{\rho}\frac{\partial^2\psi_e}{\partial\phi\partial z} + i\omega\mu\frac{\partial\psi_m}{\partial\rho} \tag{3.51}$$

$$E_z = \left(k^2 + \frac{\partial^2}{\partial z^2}\right)\psi_e \tag{3.52}$$

3.4.2 The Radial Component (E_ρ)

We treat the two terms of the operator independently.

Term 1 (TM Contribution): $\frac{\partial^2\psi_e}{\partial\rho\partial z}$ First, differentiate ψ_e with respect to z. The

spectral amplitude $\tilde{\psi}_e$ becomes $\tilde{\psi}'_e$ (where prime denotes ∂_z).

$$\frac{\partial \psi_e}{\partial z} = \sin\phi \int_0^\infty \frac{\partial \tilde{\psi}_e}{\partial z} J_1(k_\rho \rho) k_\rho \, dk_\rho \tag{3.53}$$

Next, differentiate with respect to ρ. The derivative applies only to the Bessel function $J_1(k_\rho\rho)$. Using the chain rule, $\frac{\partial}{\partial \rho} J_1(k_\rho \rho) = k_\rho J_1'(k_\rho \rho)$.

$$\text{Term 1} = \sin\phi \int_0^\infty \frac{\partial \tilde{\psi}_e}{\partial z} k_\rho J_1'(k_\rho \rho) k_\rho \, dk_\rho \tag{3.54}$$

Term 2 (TE Contribution): $-\frac{i\omega\mu}{\rho}\frac{\partial \psi_m}{\partial \phi}$ Differentiate ψ_m with respect to ϕ. Since $\psi_m \propto \cos\phi$, the derivative is $-\sin\phi$.

$$\frac{\partial \psi_m}{\partial \phi} = -\sin\phi \int_0^\infty \tilde{\psi}_m J_1(k_\rho \rho) k_\rho \, dk_\rho \tag{3.55}$$

Substitute this into the operator term:

$$\text{Term 2} = -\frac{i\omega\mu}{\rho}\left(-\sin\phi \int_0^\infty \tilde{\psi}_m J_1 k_\rho \, dk_\rho\right) = \sin\phi \int_0^\infty \frac{i\omega\mu}{\rho} \tilde{\psi}_m J_1 k_\rho \, dk_\rho \tag{3.56}$$

Total E_ρ: Summing the terms and factoring out $\sin\phi$:

$$\boxed{E_\rho = \sin\phi \int_0^\infty \left[\frac{\partial \tilde{\psi}_e}{\partial z} k_\rho J_1'(k_\rho\rho) + \frac{i\omega\mu}{\rho}\tilde{\psi}_m J_1(k_\rho\rho)\right] k_\rho \, dk_\rho} \tag{3.57}$$

3.4.3 The Azimuthal Component (E_ϕ)

Term 1 (TM Contribution): $\frac{1}{\rho}\frac{\partial^2 \psi_e}{\partial \phi \partial z}$ Differentiate ψ_e with respect to z ($\tilde{\psi}_e \to \tilde{\psi}'_e$) and ϕ ($\sin\phi \to \cos\phi$).

$$\text{Term 1} = \frac{1}{\rho}\cos\phi \int_0^\infty \frac{\partial \tilde{\psi}_e}{\partial z} J_1(k_\rho \rho) k_\rho \, dk_\rho \tag{3.58}$$

Term 2 (TE Contribution): $i\omega\mu\frac{\partial \psi_m}{\partial \rho}$ Differentiate ψ_m with respect to ρ. The derivative acts on the Bessel function: $\partial_\rho J_1(k_\rho\rho) = k_\rho J_1'(k_\rho\rho)$.

$$\text{Term 2} = i\omega\mu\cos\phi \int_0^\infty \tilde{\psi}_m k_\rho J_1'(k_\rho\rho) k_\rho \, dk_\rho \tag{3.59}$$

Total E_ϕ: Summing the terms and factoring out $\cos\phi$:

$$\boxed{E_\phi = \cos\phi \int_0^\infty \left[\frac{1}{\rho}\frac{\partial \tilde{\psi}_e}{\partial z} J_1(k_\rho \rho) + i\omega\mu\tilde{\psi}_m k_\rho J_1'(k_\rho \rho)\right] k_\rho \, dk_\rho} \tag{3.60}$$

3.4.4 The Vertical Component (E_z)

The vertical component depends only on the TM potential ψ_e.

$$E_z = \left(k^2 + \frac{\partial^2}{\partial z^2}\right)\psi_e \tag{3.61}$$

Inside the integral, the potential satisfies the homogeneous wave equation for each spectral component:

$$\left(\frac{\partial^2}{\partial z^2} + k_z^2\right)\tilde{\psi}_e(z) = 0 \implies \frac{\partial^2 \tilde{\psi}_e}{\partial z^2} = -k_z^2 \tilde{\psi}_e \tag{3.62}$$

Substituting this into the operator:

$$k^2 + \frac{\partial^2}{\partial z^2} \to k^2 - k_z^2 \tag{3.63}$$

From the dispersion relation $k_z^2 = k^2 - k_\rho^2$, we have $k^2 - k_z^2 = k_\rho^2$. Therefore, the operator simplifies to multiplication by the squared radial wavenumber k_ρ^2.

Total E_z:

$$\boxed{E_z = \sin\phi \int_0^\infty \left[k_\rho^2 \tilde{\psi}_e(z)\right] J_1(k_\rho \rho) k_\rho \, dk_\rho} \tag{3.64}$$

This derivation confirms that the vertical electric field is directly proportional to the squared radial wavenumber of the TM potential.

3.5 Magnetic Field Components (H_ρ, H_ϕ, H_z)

Following the derivation of the electric field components, we now derive the explicit spectral integral expressions for the magnetic field components. These are critical for determining the input impedance of the antenna and for matching boundary conditions at the interfaces.

3.5.1 Potentials and Operators

We utilize the same spectral definitions for the Hertz potentials in layer j:

$$\psi_e(\rho, \phi, z) = \sin\phi \int_0^\infty \tilde{\psi}_e(z, k_\rho) J_1(k_\rho \rho) k_\rho \, dk_\rho \tag{3.65}$$

$$\psi_m(\rho, \phi, z) = \cos\phi \int_0^\infty \tilde{\psi}_m(z, k_\rho) J_1(k_\rho \rho) k_\rho \, dk_\rho \tag{3.66}$$

Recall that for the magnetic field, the general operators derived from the curl-curl relations (Section 3.3) are:

$$H_\rho = \frac{\partial^2 \psi_m}{\partial \rho \partial z} - \frac{i\omega\hat{\epsilon}}{\rho} \frac{\partial \psi_e}{\partial \phi} \tag{3.67}$$

$$H_\phi = \frac{1}{\rho} \frac{\partial^2 \psi_m}{\partial \phi \partial z} + i\omega\hat{\epsilon} \frac{\partial \psi_e}{\partial \rho} \tag{3.68}$$

$$H_z = \left(k^2 + \frac{\partial^2}{\partial z^2}\right) \psi_m \tag{3.69}$$

Note that $\hat{\epsilon}$ is the complex permittivity of the layer, accounting for conductivity losses.

3.5.2 The Radial Component (H_ρ)

Term 1 (TE Contribution): $\frac{\partial^2 \psi_m}{\partial \rho \partial z}$ First, differentiate ψ_m with respect to z ($\tilde{\psi}_m \to \tilde{\psi}'_m$). Then, differentiate with respect to ρ. Since $\psi_m \propto \cos\phi$:

$$\text{Term 1} = \cos\phi \int_0^\infty \frac{\partial \tilde{\psi}_m}{\partial z} k_\rho J_1'(k_\rho \rho) k_\rho \, dk_\rho \tag{3.70}$$

Term 2 (TM Contribution): $-\frac{i\omega\hat{\epsilon}}{\rho} \frac{\partial \psi_e}{\partial \phi}$ Differentiate ψ_e with respect to ϕ. Since $\psi_e \propto \sin\phi$, the derivative is $\cos\phi$.

$$\frac{\partial \psi_e}{\partial \phi} = \cos\phi \int_0^\infty \tilde{\psi}_e J_1(k_\rho \rho) k_\rho \, dk_\rho \tag{3.71}$$

Substituting this into the operator:

$$\text{Term 2} = -\frac{i\omega\hat{\epsilon}}{\rho} \cos\phi \int_0^\infty \tilde{\psi}_e J_1 k_\rho \, dk_\rho \tag{3.72}$$

Total H_ρ: Summing the terms and factoring out $\cos\phi$:

$$\boxed{H_\rho = \cos\phi \int_0^\infty \left[\frac{\partial \tilde{\psi}_m}{\partial z} k_\rho J_1'(k_\rho \rho) - \frac{i\omega\hat{\epsilon}}{\rho} \tilde{\psi}_e J_1(k_\rho \rho) \right] k_\rho \, dk_\rho} \tag{3.73}$$

3.5.3 The Azimuthal Component (H_ϕ)

Term 1 (TE Contribution): $\frac{1}{\rho}\frac{\partial^2 \psi_m}{\partial \phi \partial z}$ Differentiate ψ_m with respect to z ($\tilde{\psi}_m \to \tilde{\psi}'_m$) and ϕ. Since $\psi_m \propto \cos\phi$, the angular derivative is $-\sin\phi$.

$$\text{Term 1} = \frac{1}{\rho}(-\sin\phi)\int_0^\infty \frac{\partial \tilde{\psi}_m}{\partial z} J_1(k_\rho \rho) k_\rho \, dk_\rho \tag{3.74}$$

Term 2 (TM Contribution): $i\omega\hat{\epsilon}\frac{\partial \psi_e}{\partial \rho}$ Differentiate ψ_e with respect to ρ. The derivative yields $k_\rho J_1'(k_\rho \rho)$.

$$\text{Term 2} = i\omega\hat{\epsilon}\sin\phi \int_0^\infty \tilde{\psi}_e k_\rho J_1'(k_\rho \rho) k_\rho \, dk_\rho \tag{3.75}$$

Total H_ϕ: Summing the terms and factoring out $\sin\phi$:

$$\boxed{H_\phi = \sin\phi \int_0^\infty \left[-\frac{1}{\rho}\frac{\partial \tilde{\psi}_m}{\partial z} J_1(k_\rho \rho) + i\omega\hat{\epsilon}\tilde{\psi}_e k_\rho J_1'(k_\rho \rho) \right] k_\rho \, dk_\rho} \tag{3.76}$$

3.5.4 The Vertical Component (H_z)

The vertical magnetic field depends exclusively on the TE potential ψ_m.

$$H_z = \left(k^2 + \frac{\partial^2}{\partial z^2}\right)\psi_m \tag{3.77}$$

Similar to the derivation of E_z, we substitute the spectral wave equation $\frac{\partial^2 \tilde{\psi}_m}{\partial z^2} = -k_z^2 \tilde{\psi}_m$. Using the dispersion relation $k^2 - k_z^2 = k_\rho^2$, the operator reduces to multiplication by k_ρ^2.

Total H_z:

$$\boxed{H_z = \cos\phi \int_0^\infty \left[k_\rho^2 \tilde{\psi}_m(z)\right] J_1(k_\rho \rho) k_\rho \, dk_\rho} \tag{3.78}$$

3.5.5 Summary of Angular Dependencies

The derivations in Section 3.4 and 3.5 confirm the fundamental symmetry of the Horizontal Magnetic Dipole fields:

- $\sin\phi$ **dependence:** E_ρ, E_z, H_ϕ
- $\cos\phi$ **dependence:** E_ϕ, H_ρ, H_z

This angular separation is utilized in the computational code to compute the fields along a single radial cut (e.g., $\phi = 0$ or $\phi = \pi/2$) and then reconstruct the full 3D field analytically.

Chapter 4

Boundary Conditions and Global Matrix Method

4.1 Electromagnetic Boundary Conditions

Consider an interface at depth $z = z_j$ separating layer j (medium parameters $\epsilon_j, \mu_j, \sigma_j$) from layer $j+1$ (parameters $\epsilon_{j+1}, \mu_{j+1}, \sigma_{j+1}$). The fundamental boundary conditions for time-harmonic fields in the absence of surface currents require the continuity of the tangential field components across the interface:

$$\hat{z} \times (\mathbf{E}_{j+1} - \mathbf{E}_j)\big|_{z=z_j} = 0, \quad \hat{z} \times (\mathbf{H}_{j+1} - \mathbf{H}_j)\big|_{z=z_j} = 0 \tag{4.1}$$

In the cylindrical coordinate system, these vector equations imply the continuity of four scalar components: E_ρ, E_ϕ, H_ρ, and H_ϕ.

4.1.1 Tangential Electric Field Continuity

We first apply the continuity condition to the tangential electric field components. Using the spectral expressions derived in Eq. (3.54) and Eq. (3.57), the continuity of E_ϕ at $z = z_j$ is written as:

$$E_{\phi,j}(\rho, \phi, z_j) = E_{\phi,j+1}(\rho, \phi, z_j) \tag{4.2}$$

Substituting the integral forms:

$$\begin{aligned}\cos\phi \int_0^\infty \left[\frac{ik_{zj}}{\rho}(-A_j\xi_j^- + B_j\xi_j^+)J_1(k_\rho\rho) + i\omega\mu_j(C_j\xi_j^- + D_j\xi_j^+)k_\rho J_1'(k_\rho\rho)\right] k_\rho\, dk_\rho \\ = \cos\phi \int_0^\infty \left[\frac{ik_{z,j+1}}{\rho}(-A_{j+1}\xi_{j+1}^- + B_{j+1}\xi_{j+1}^+)J_1(k_\rho\rho) + \dots\right] k_\rho\, dk_\rho\end{aligned} \tag{4.3}$$

where we have introduced the shorthand for the phase terms at the boundary:

$$\xi_j^- = e^{-ik_{zj}z_j}, \quad \xi_j^+ = e^{ik_{zj}z_j} \tag{4.4}$$

For this equality to hold for all values of ρ, the integrands must match. Furthermore, since the functions $J_1(k_\rho\rho)$ and $J_1'(k_\rho\rho)$ are linearly independent, their coefficients must be equated independently.

1. Matching the TE terms (coefficients of J_1'): The terms associated with J_1' in the E_ϕ expression correspond to the magnetic potential ψ_m (TE mode). Equating these yields:

$$i\omega\mu_j(C_j\xi_j^- + D_j\xi_j^+) = i\omega\mu_{j+1}(C_{j+1}\xi_{j+1}^- + D_{j+1}\xi_{j+1}^+) \tag{4.5}$$

Dividing by $i\omega$, we obtain the first working equation:

$$\mu_j(C_j e^{-ik_{zj}z_j} + D_j e^{ik_{zj}z_j}) = \mu_{j+1}(C_{j+1}e^{-ik_{z,j+1}z_j} + D_{j+1}e^{ik_{z,j+1}z_j}) \tag{4.6}$$

2. Matching the TM terms (coefficients of J_1): The terms associated with J_1 in the E_ϕ expression correspond to the electric potential ψ_e (TM mode). Equating these yields:

$$\frac{ik_{zj}}{\rho}(-A_j\xi_j^- + B_j\xi_j^+) = \frac{ik_{z,j+1}}{\rho}(-A_{j+1}\xi_{j+1}^- + B_{j+1}\xi_{j+1}^+) \tag{4.7}$$

Canceling common terms (i/ρ), we obtain the second working equation:

$$k_{zj}(-A_j e^{-ik_{zj}z_j} + B_j e^{ik_{zj}z_j}) = k_{z,j+1}(-A_{j+1}e^{-ik_{z,j+1}z_j} + B_{j+1}e^{ik_{z,j+1}z_j}) \tag{4.8}$$

Note: Applying the continuity condition to E_ρ yields these exact same two equations, confirming the consistency of the formulation.

4.1.2 Tangential Magnetic Field Continuity

Next, we apply the continuity condition to the tangential magnetic field components, H_ρ and H_ϕ.

$$H_{\phi,j}(\rho,\phi,z_j) = H_{\phi,j+1}(\rho,\phi,z_j) \tag{4.9}$$

Using the explicit integrals from Eq. (3.64), we again separate the terms based on their Bessel function dependence (J_1 vs J_1').

1. Matching the TM terms (coefficients of J_1'): The terms associated with J_1' in the H_ϕ expression involve the complex permittivity $\hat{\epsilon}$.

$$-i\omega\hat{\epsilon}_j(A_j\xi_j^- + B_j\xi_j^+) = -i\omega\hat{\epsilon}_{j+1}(A_{j+1}\xi_{j+1}^- + B_{j+1}\xi_{j+1}^+) \tag{4.10}$$

This simplifies to the third working equation:

$$\hat{\epsilon}_j(A_j e^{-ik_{zj}z_j} + B_j e^{ik_{zj}z_j}) = \hat{\epsilon}_{j+1}(A_{j+1}e^{-ik_{z,j+1}z_j} + B_{j+1}e^{ik_{z,j+1}z_j}) \tag{4.11}$$

2. Matching the TE terms (coefficients of J_1): The terms associated with J_1 in the H_ϕ expression involve the vertical derivative of the magnetic potential.

$$\frac{ik_{zj}}{\rho}(-C_j\xi_j^- + D_j\xi_j^+) = \frac{ik_{z,j+1}}{\rho}(-C_{j+1}\xi_{j+1}^- + D_{j+1}\xi_{j+1}^+) \tag{4.12}$$

This yields the fourth and final working equation for this interface:

$$k_{zj}(-C_j e^{-ik_{zj}z_j} + D_j e^{ik_{zj}z_j}) = k_{z,j+1}(-C_{j+1}e^{-ik_{z,j+1}z_j} + D_{j+1}e^{ik_{z,j+1}z_j}) \tag{4.13}$$

Summary of Interface Equations: For every interface $j = 1 \dots N-1$, we have derived four linear algebraic equations (Eqs. 4.6, 4.8, 4.11, 4.13). These equations couple the unknown wave amplitudes of layer j to those of layer $j+1$. In the next section, we will organize these equations into matrix blocks to solve for the global system.

4.2 Method Selection

The theoretical formulation presented in the preceding chapters establishes the Global Matrix Method (GMM) as a rigorous analytical framework for solving the electromagnetic field in stratified media. However, the resulting solution is expressed in the spectral domain as a semi-infinite Sommerfeld integral of the form:

$$I(\rho, z) = \int_0^\infty F(\lambda, z) J_m(\lambda\rho)\, d\lambda \tag{4.14}$$

This integral cannot be solved analytically for lossy media such as seawater. Therefore, a robust numerical strategy is required to transform these spectral solutions into observable spatial fields.

In computational electromagnetics, two primary classes of methods are available for this task:

1. **Domain Discretization Methods:** Such as the Finite Element Method (FEM) or Finite Difference Time Domain (FDTD), which mesh the entire physical volume.

2. **Spectral Integration Methods:** Such as the Fast Hankel Transform (FHT) or direct quadrature integration of the Global Matrix solution.

This Section first presents a comparative study of FEM to justify why it was not selected for this specific research. Subsequently, we detail the implementation of the chosen spectral approach—specifically, the Romberg-Shanks composite integration algorithm—which offers superior efficiency for the stratified ocean models considered in this thesis.

4.3 Comparative Study: The Finite Element Method (FEM)

While the Global Matrix Method (GMM) is the primary focus of this thesis, it is essential to contextualize this approach against the Finite Element Method (FEM)[21], which is the standard technique for modeling complex, arbitrary geometries. This section outlines the formulation of FEM and demonstrates why it is computationally less efficient than GMM for the specific case of stratified planar media.

4.3.1 Weak Formulation of the Helmholtz Equation

Unlike the GMM, which solves the wave equation in the spectral (wavenumber) domain, FEM solves the problem in the spatial domain by discretizing the physical volume. We begin with the vector Helmholtz equation derived in Chapter 2:

$$\nabla \times \left(\frac{1}{\mu_r} \nabla \times \mathbf{E} \right) - k_0^2 \epsilon_r \mathbf{E} = -i\omega\mu_0 \mathbf{J} \tag{4.15}$$

To apply FEM, we must convert this differential equation into its "weak" or integral form. We multiply by a vector testing function $\mathbf{W}$ and integrate over the volume V:

$$\iiint_V \left[(\nabla \times \mathbf{W}) \cdot \left(\frac{1}{\mu_r} \nabla \times \mathbf{E} \right) - k_0^2 \epsilon_r \mathbf{W} \cdot \mathbf{E} \right] dV = -i\omega\mu_0 \iiint_V \mathbf{W} \cdot \mathbf{J} dV \tag{4.16}$$

This formulation allows for the modeling of inhomogeneous geometries where parameters ϵ and σ vary arbitrarily in 3D space, rather than being restricted to horizontal layers.

4.3.2 Discretization and Basis Functions

In FEM, the continuous solution domain is subdivided into a mesh of finite elements (typically tetrahedra or hexahedra). Within each element, the unknown electric field

$\mathbf{E}$ is approximated as a summation of basis functions $\mathbf{N}_i$:

$$\mathbf{E}(\mathbf{r}) \approx \sum_{j=1}^{M} e_j \mathbf{N}_j(\mathbf{r}) \tag{4.17}$$

where e_j are the unknown coefficients. This discretization reduces the continuous operator into a sparse linear matrix system:

$$[\mathbf{K}]\{e\} = \{b\} \tag{4.18}$$

Here, $[\mathbf{K}]$ is the stiffness matrix representing the geometry and material properties, and $\{b\}$ is the excitation vector.

4.3.3 Comparative Analysis: GMM vs. FEM

For the specific problem of a dipole submerged in stratified seawater, the Global Matrix Method offers distinct advantages over FEM. A comparison of the two approaches is presented in Table 4.1.

Table 4.1: Comparison of Computational Methods for Marine EM Modeling.

Feature	**Global Matrix Method (GMM)**	**Finite Element Method (FEM)**
Domain	Spectral Wavenumber (k_ρ, z)	Spatial Volume (x, y, z)
Geometry	Infinite Horizontal Layers	Arbitrary 3D Geometries
Boundaries	Analytical (Exact for $\rho \to \infty$)	Requires Absorbing Boundary Conditions (ABC/PML) to simulate infinity
Accuracy	Semi-analytical (Exact in z)	Approximation (Dependent on mesh density)
Efficiency	**High** for layered media	**Low** for large open oceans (requires massive memory)

4.3.4 Selection Justification

While FEM is superior for modeling complex seafloor topographies (e.g., seamounts or pipelines), it suffers from "numerical dispersion" and requires computationally expensive Absorbing Boundary Conditions (ABC) to simulate an infinite ocean.

In contrast, the Global Matrix Method treats the horizontal layers as infinite by definition. Since this thesis focuses on the fundamental mode propagation in a flat, stratified ocean, the GMM provides a solution that is both faster and free from mesh-discretization errors. Consequently, the remainder of this chapter focuses on the numerical implementation of the spectral GMM integrals.

In the previous chapter, we derived the spectral integral representations of the electromagnetic field components in an arbitrary layer j. These expressions contain unknown amplitude coefficients: A_j and B_j for the Transverse Magnetic (TM) mode, and C_j and D_j for the Transverse Electric (TE) mode.

To solve for these unknowns, we employ the Global Matrix Method(GMM). This technique assembles the boundary conditions at every interface into a single, comprehensive linear system. This chapter details the construction of the global matrix and the solution procedure for the stratified media model.

4.4 Formulation of the Interface Matrices

To implement the Global Matrix Method numerically, we must explicitly define the entries of the local sub-matrices $\mathbf{D}_j$ and $\mathbf{U}_{j+1}$ that constitute the global system.

Recall the state vector for layer j is ordered as $\mathbf{X}_j = [A_j, B_j, C_j, D_j]^T$. The rows of the matrix correspond to the four boundary conditions derived in Section 5.1. For stability and clarity, we group the Transverse Magnetic (TM) equations first, followed by the Transverse Electric (TE) equations.

4.4.1 Matrix Rows Definition

The four rows of the local matrix system at interface z_j correspond to:

1. Row 1: Continuity of TM Electric Potential derivative (from E_ρ/E_ϕ matching).
2. Row 2: Continuity of TM Magnetic Potential (from H_ϕ matching).
3. Row 3: Continuity of TE Magnetic Potential (from E_ϕ matching).
4. Row 4: Continuity of TE Electric Potential derivative (from H_ρ/H_ϕ matching).

4.4.2 The Local Layer Matrix ($\mathbf{D}_j$)

The matrix $\mathbf{D}_j$ represents the contribution of layer j (the layer above the interface) to the boundary conditions at $z = z_j$. Let $\xi_j^- = e^{-ik_{zj}z_j}$ (down-going phase) and $\xi_j^+ = e^{ik_{zj}z_j}$ (up-going phase).

$$\mathbf{D}_j = \begin{bmatrix} -k_{zj}\xi_j^- & k_{zj}\xi_j^+ & 0 & 0 \\ \hat{\epsilon}_j\xi_j^- & \hat{\epsilon}_j\xi_j^+ & 0 & 0 \\ 0 & 0 & \mu_j\xi_j^- & \mu_j\xi_j^+ \\ 0 & 0 & -k_{zj}\xi_j^- & k_{zj}\xi_j^+ \end{bmatrix} \tag{4.19}$$

4.4.3 The Upper Layer Matrix ($\mathbf{U}_{j+1}$)

The matrix $\mathbf{U}_{j+1}$ represents the contribution of layer $j+1$ (the layer below the interface) to the boundary conditions at $z = z_j$. Since the standard form is $\mathbf{D}_j\mathbf{X}_j - \mathbf{U}_{j+1}\mathbf{X}_{j+1} = 0$ (or similar depending on sign convention), we move these terms to the same side of the equation as $\mathbf{D}_j$. This effectively negates the coefficients derived in Section 5.1.

Let $\xi^-_{j+1} = e^{-ik_{z,j+1}z_j}$ and $\xi^+_{j+1} = e^{ik_{z,j+1}z_j}$.

$$\mathbf{U}_{j+1} = \begin{bmatrix} -(-k_{z,j+1}\xi^-_{j+1}) & -(k_{z,j+1}\xi^+_{j+1}) & 0 & 0 \\ -(\hat{\epsilon}_{j+1}\xi^-_{j+1}) & -(\hat{\epsilon}_{j+1}\xi^+_{j+1}) & 0 & 0 \\ 0 & 0 & -(\mu_{j+1}\xi^-_{j+1}) & -(\mu_{j+1}\xi^+_{j+1}) \\ 0 & 0 & -(-k_{z,j+1}\xi^-_{j+1}) & -(k_{z,j+1}\xi^+_{j+1}) \end{bmatrix} \tag{4.20}$$

Simplifying the signs:

$$\mathbf{U}_{j+1} = \begin{bmatrix} k_{z,j+1}\xi^-_{j+1} & -k_{z,j+1}\xi^+_{j+1} & 0 & 0 \\ -\hat{\epsilon}_{j+1}\xi^-_{j+1} & -\hat{\epsilon}_{j+1}\xi^+_{j+1} & 0 & 0 \\ 0 & 0 & -\mu_{j+1}\xi^-_{j+1} & -\mu_{j+1}\xi^+_{j+1} \\ 0 & 0 & k_{z,j+1}\xi^-_{j+1} & -k_{z,j+1}\xi^+_{j+1} \end{bmatrix} \tag{4.21}$$

4.4.4 Special Case: The Source Vector Coupling

As noted in Section 3.2, the source vector $\mathbf{S}$ arises because the TE potential in the source layer (s) contains the primary field term S^{prim}. For the interface z_s (bottom of the source layer), the boundary condition equation for the TE magnetic potential (Row 3) becomes:

$$\mu_s(C_s\xi^-_s + D_s\xi^+_s) - \mu_{s+1}(C_{s+1}\xi^-_{s+1} + D_{s+1}\xi^+_{s+1}) = -\mu_s(S^{prim}_s(z_s)) \tag{4.22}$$

where $S^{prim}_s(z_s) = \frac{M_0}{4\pi\omega\mu_s}\frac{1}{k_{zs}}e^{ik_{zs}|z_s - z_{source}|}$.

Similar adjustments are made for Row 4 (TE Electric Potential derivative), where the derivative of the primary field introduces a factor of ik_{zs} (or $-ik_{zs}$ depending on direction). The TM rows (1 and 2) in the source vector remain zero because the HMD is purely a magnetic source in the vertical sense ($\Pi^{prim}_e = 0$).

This formulation allows us to construct the sparse global matrix row-by-row, ensuring that the coupling between layers is handled exactly for both TE and TM modes.

4.4.5 TM Mode Matrices

As demonstrated in Section 4.1, the boundary conditions for the Transverse Magnetic mode (involving coefficients A_j, B_j) can be satisfied independently of the Transverse Electric mode. This allows us to construct a dedicated TM Global Matrix.

The local state vector for the TM mode in layer j is $\mathbf{X}_j^{TM} = [A_j, B_j]^T$. The boundary conditions enforced are:

1. Continuity of H_ϕ: Requires continuity of $\hat{\epsilon}\psi_e$.
2. Continuity of E_ϕ: Requires continuity of $\frac{\partial \psi_e}{\partial z}$ (or equivalently $k_z\psi_e$).

Defining the phase terms $\xi_j^- = e^{-ik_{zj}z_j}$ and $\xi_j^+ = e^{ik_{zj}z_j}$, the local matrix $\mathbf{D}_j^{TM}$ (layer above the interface) is:

$$\mathbf{D}_j^{TM} = \begin{bmatrix} \hat{\epsilon}_j\xi_j^- & \hat{\epsilon}_j\xi_j^+ \\ -k_{zj}\xi_j^- & k_{zj}\xi_j^+ \end{bmatrix} \tag{4.23}$$

The matrix $\mathbf{U}_{j+1}^{TM}$ (layer below the interface), with signs adjusted to move to the left-hand side of the equation ($\mathbf{D}\mathbf{X}_j - \mathbf{U}\mathbf{X}_{j+1} = 0$), is:

$$\mathbf{U}_{j+1}^{TM} = \begin{bmatrix} \hat{\epsilon}_{j+1}\xi_{j+1}^- & \hat{\epsilon}_{j+1}\xi_{j+1}^+ \\ -k_{z,j+1}\xi_{j+1}^- & k_{z,j+1}\xi_{j+1}^+ \end{bmatrix} \tag{4.24}$$

4.4.6 TE Mode Matrices

Similarly, the Transverse Electric mode (involving coefficients C_j, D_j) forms an independent system. The local state vector is $\mathbf{X}_j^{TE} = [C_j, D_j]^T$. The boundary conditions enforced are:

1. Continuity of E_ϕ: Requires continuity of $\mu\psi_m$.
2. Continuity of H_ϕ: Requires continuity of $\frac{\partial \psi_m}{\partial z}$.

The local matrix $\mathbf{D}_j^{TE}$ (layer above the interface) is:

$$\mathbf{D}_j^{TE} = \begin{bmatrix} \mu_j\xi_j^- & \mu_j\xi_j^+ \\ -k_{zj}\xi_j^- & k_{zj}\xi_j^+ \end{bmatrix} \tag{4.25}$$

The matrix $\mathbf{U}_{j+1}^{TE}$ (layer below the interface) is:

$$\mathbf{U}_{j+1}^{TE} = \begin{bmatrix} \mu_{j+1}\xi_{j+1}^- & \mu_{j+1}\xi_{j+1}^+ \\ -k_{z,j+1}\xi_{j+1}^- & k_{z,j+1}\xi_{j+1}^+ \end{bmatrix} \tag{4.26}$$

Implication for Numerical Solution

By decoupling the system, we solve two smaller block-diagonal matrix equations of size $2N \times 2N$ instead of one large $4N \times 4N$ system.

$$\mathbf{M}^{TM}\mathbf{X}^{TM} = \mathbf{0} \quad \text{(Since HMD implies } \Pi_e^{prim} = 0\text{)} \tag{4.27}$$

$$\mathbf{M}^{TE}\mathbf{X}^{TE} = \mathbf{S}^{TE} \tag{4.28}$$

While the primary potential Π_e^{prim} is zero, the HMD source **does** excite the TM mode through the boundary coupling if the layers have different electromagnetic properties. However, in the strict formulation where boundaries decouple J_1 and J_1' terms, the source vector $\mathbf{S}^{TM}$ is zero only if the source itself does not project onto the TM basis. For the Horizontal Magnetic Dipole, the source is purely magnetic (TE) in nature. The TM fields arise solely from mode conversion at boundaries in non-horizontal setups, or if the source term H_z^{prim} forces a response. In this specific orthogonal spectral formulation, the HMD source term appears strictly in the TE equations ($\mathbf{S}^{TE}$).

4.5 Modeling the Source: The Dummy Interface

The Global Matrix Method relies on matching wave amplitudes at layer interfaces. However, the source (Horizontal Magnetic Dipole) is typically located at a depth z_s within a homogeneous layer, not necessarily at a physical boundary.

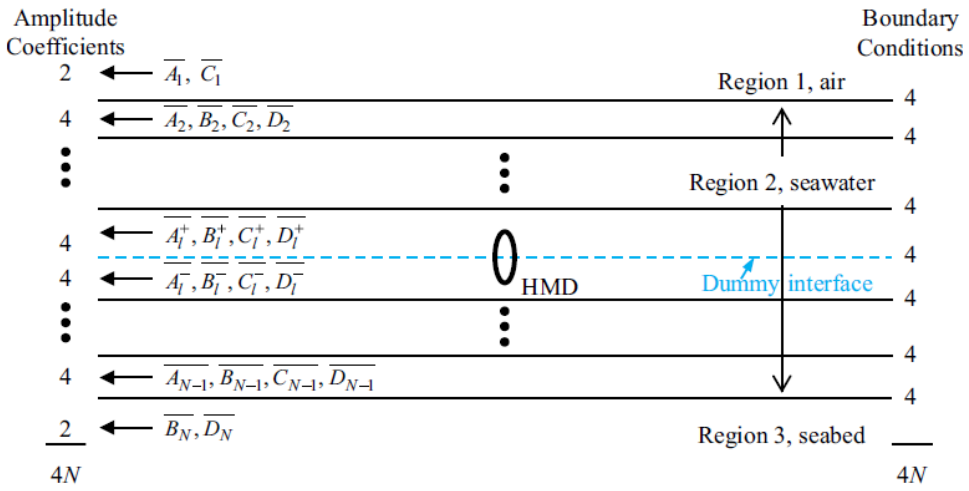

Figure 4.1: Equivalent transmission line network representing the wave propagation and reflection coefficients at each interface of the stratified medium[8].

To incorporate the source singularity into the matrix formalism, we introduce a Dummy Interface at $z = z_s$. This technique effectively splits the physical source layer

(let's denote it as layer s) into two sub-layers:

- Layer s (Upper): Extends from the physical interface z_{s-1} down to the source depth z_s.
- Layer $s+1$ (Lower): Extends from the source depth z_s down to the physical interface z_{s+1}.

Both sub-layers possess identical material properties $(\epsilon_s, \mu_s, \sigma_s)$. The "jump" in the electromagnetic field caused by the source current is then applied as a boundary condition at this dummy interface.

4.5.1 Jump Conditions at the Source Depth

At the dummy interface $z = z_s$, the total electromagnetic field is the superposition of the continuous secondary field (scattered from other layers) and the singular primary field generated by the dipole.

Mathematically, we require the total tangential fields to be continuous. However, it is more convenient to formulate the boundary condition in terms of the unknown wave amplitudes $\mathbf{X}$. The discontinuity arises because the primary field radiates outwards from z_s in opposite directions (up-going for $z < z_s$, down-going for $z > z_s$).

Let the primary magnetic potential be ψ_m^{prim}. From the Sommerfeld identity (Section 4.2), the spectral behavior is:

$$\tilde{\psi}_m^{prim}(k_\rho, z) \propto e^{ik_{zs}|z-z_s|} \tag{4.29}$$

- At $z = z_s^+$ (just below): The wave travels downwards ($\propto e^{ik_{zs}z}$).
- At $z = z_s^-$ (just above): The wave travels upwards ($\propto e^{-ik_{zs}z}$).

While the potential itself is continuous at z_s, its vertical derivative $\frac{\partial \psi_m}{\partial z}$ exhibits a discontinuity (jump) proportional to the source strength.

The boundary conditions at the dummy interface can be written as:

$$\mathbf{D}_s\mathbf{X}_s - \mathbf{U}_{s+1}\mathbf{X}_{s+1} = \mathbf{J}_s \tag{4.30}$$

where $\mathbf{J}_s$ is the Jump Vector representing the difference in the primary field components across the interface.

4.5.2 The Source Excitation Vector

The jump vector $\mathbf{J}_s$ forms the non-zero entries of the global source vector $\mathbf{S}$. For a Horizontal Magnetic Dipole, the source is purely magnetic in nature (TE excitation), but due to the coupling in the boundary conditions, we must be careful.

Recall the magnitude of the primary potential from Section 4.1: $S_0 = \frac{M_0}{4\pi\omega\mu_s}\frac{k_\rho}{k_{zs}}$. The jump conditions for the four matrix rows at z_s are:

1. TM Mode Rows (Rows 1 & 2): Since the HMD is a magnetic loop, it does not possess a primary electric vertical potential ($\psi_e^{prim} = 0$). Therefore, there is no jump in the TM quantities.

$$J_s^{(1)} = 0, \quad J_s^{(2)} = 0 \tag{4.31}$$

2. TE Mode Rows (Rows 3 & 4): The TE rows enforce continuity of $\mu\psi_m$ and $\frac{\partial\psi_m}{\partial z}$.

- Row 3 (Continuity of ψ_m): The primary potential is continuous at the source ($e^0 = e^0 = 1$).

$$\psi_m^{prim}(z_s^+) - \psi_m^{prim}(z_s^-) = S_0 - S_0 = 0 \tag{4.32}$$

  Wait, this is zero only if we strictly view it as continuity. However, in the matrix $\mathbf{MX} = \mathbf{S}$, the vector $\mathbf{X}$ contains the 'secondary' amplitudes (or total amplitudes 'minus' the primary). Usually, we solve for the total amplitudes. In this case, the coefficients C_s, D_s (layer above) and C_{s+1}, D_{s+1} (layer below) must account for the fact that the "down-going" wave in the lower layer includes the source, while the "down-going" wave in the upper layer does not.

  The standard approach is to effectively inject the source term S_0 into the appropriate slots of the RHS vector $\mathbf{S}$.

- Row 4 (Continuity of $\partial_z\psi_m$):

$$\frac{\partial}{\partial z}\psi_m^{prim}(z_s^+) = ik_{zs}S_0 \quad \text{(Down-going)} \tag{4.33}$$

$$\frac{\partial}{\partial z}\psi_m^{prim}(z_s^-) = -ik_{zs}S_0 \quad \text{(Up-going)} \tag{4.34}$$

  The jump is $ik_{zs}S_0 - (-ik_{zs}S_0) = 2ik_{zs}S_0$.

Thus, the source excitation vector $\mathbf{S}$ for the global system $\mathbf{MX} = \mathbf{S}$ is strictly zero everywhere except at the indices corresponding to the dummy interface equations. For the interface at z_s:

$$\mathbf{S}_{local} = \begin{bmatrix} 0 \\ 0 \\ 0 \\ 2ik_{zs}S_0 \end{bmatrix} = \begin{bmatrix} 0 \\ 0 \\ 0 \\ \frac{M_0 k_\rho}{2\pi\omega\mu_s} \end{bmatrix} \tag{4.35}$$

By placing this term in the global vector, the linear solver automatically propagates the energy from the dipole into all layers, converting it into TE and TM modes via reflection and refraction at the physical boundaries.

4.6 Radiation Conditions at Infinity

The general solution for the wave equation in any layer j contains both down-going waves (amplitudes A_j, C_j) and up-going waves (amplitudes B_j, D_j). While this superposition is valid for all bounded internal layers, the semi-infinite half-spaces at the top and bottom of the model require special physical constraints known as "Radiation Conditions".

These conditions ensure that in the unbounded regions, energy propagates only away from the source (scattering region) and does not originate from infinity.

4.6.1 Upper Half-Space (Layer 0)

The upper half-space (Layer 0) represents the region $z < z_0$ (typically the air or the upper atmosphere). We assume there are no sources located at $z \to -\infty$. Consequently, there can be no wave energy traveling in the positive z-direction (downward) originating from negative infinity. Mathematically, this requires the coefficients of the down-going spectral components to vanish.

For the Transverse Magnetic (TM) mode:

$$A_0 = 0 \tag{4.36}$$

For the Transverse Electric (TE) mode:

$$C_0 = 0 \tag{4.37}$$

Thus, the electromagnetic field in Layer 0 is described purely by up-going waves (coefficients B_0, D_0) moving away from the ocean surface.

$$\psi_{e,0} \propto B_0 e^{ik_{z0}z}, \quad \psi_{m,0} \propto D_0 e^{ik_{z0}z} \tag{4.38}$$

(assuming the sign convention where $e^{ik_{z0}z}$ with $z < 0$ represents upward travel for $e^{-i\omega t}$ time dependence).

4.6.2 Lower Half-Space (Layer N)

The lower half-space (Layer N) represents the seabed basement or the Earth's crust, extending to $z \to +\infty$. Similarly, we assume no sources exist deep within the earth sending energy upwards. Therefore, there can be no wave energy traveling in the negative z-direction (upward) originating from positive infinity. The coefficients of the up-going spectral components must vanish.

For the TM mode:

$$B_N = 0 \tag{4.39}$$

For the TE mode:

$$D_N = 0 \tag{4.40}$$

The field in the basement is described purely by down-going waves (coefficients A_N, C_N) radiating into the earth.

$$\psi_{e,N} \propto A_N e^{-ik_{zN}z}, \quad \psi_{m,N} \propto C_N e^{-ik_{zN}z} \tag{4.41}$$

4.6.3 Reduction of the Global System

These radiation conditions significantly reduce the computational size of the problem.

- Standard Layers $(2 \dots N-1)$: 4 unknowns per layer (A, B, C, D).
- Layer 1: Reduced to 2 unknowns (B_0, D_0).
- Layer N: Reduced to 2 unknowns (A_N, C_N).

This reduction is implemented directly in the global matrix $\mathbf{M}$ by modifying the dimensions of the corner blocks.

- The first matrix block $\mathbf{D}_0$ (associated with Interface 0) becomes a 4×2 matrix, multiplying the vector $[B_0, D_0]^T$.
- The last matrix block $\mathbf{U}_N$ (associated with Interface $N-1$) becomes a 4×2 matrix, multiplying the vector $[A_N, C_N]^T$.

By enforcing these conditions, we ensure the uniqueness of the solution and guarantee that the Global Matrix is non-singular (invertible), provided the physical parameters are distinct.

4.7 Assembly of the Global Matrix System

With the local interface matrices defined and the boundary conditions established, we can now assemble the full linear system. The goal is to construct the global sparse matrix $\mathbf{M}$ and the source vector $\mathbf{S}$ such that the equation $\mathbf{MX} = \mathbf{S}$ can be solved for the unknown field amplitudes $\mathbf{X}$.

4.7.1 Structure of the Global Matrix

The global matrix $\mathbf{M}$ is a block-bidiagonal matrix. For a stratified medium with N layers (Layer 1 to Layer N), there are N interfaces.

If we treat the TE and TM modes as decoupled systems (as justified in Section 3.2), we form two independent matrices, each of size $2N \times 2N$. Let us consider the general case where we assemble the matrix for one mode (e.g., TE).

The rows of $\mathbf{M}$ correspond to the continuity equations at each interface j ($j = 1 \dots N-1$). The columns correspond to the unknown wave amplitudes in each layer. The assembly proceeds by iterating through the interfaces from top ($j = 1$) to bottom ($j = N-1$).

$$\mathbf{M} = \begin{bmatrix} \mathbf{D}_0^* & \mathbf{U}_1 & 0 & \dots & 0 \\ 0 & \mathbf{D}_1 & \mathbf{U}_2 & \dots & 0 \\ \vdots & \vdots & \ddots & \vdots & \vdots \\ 0 & \dots & \mathbf{D}_{N-1} & \mathbf{U}_N^* & \end{bmatrix} \tag{4.42}$$

Handling Radiation Conditions (The Corner Blocks)

The first and last diagonal blocks require special handling to incorporate the radiation conditions derived in Section 4.4.

1. Top Interface ($j = 0$): Layer 0 (upper half-space) only has up-going waves. The unknown vector for Layer 0 is reduced to a single component per mode (e.g., B_0 for TM, D_0 for TE). Therefore, the matrix block $\mathbf{D}_0^*$ is a 2×1 column vector (instead of 2×2):

   $$\mathbf{D}_0^* = \begin{bmatrix} (\mathbf{D}_0)_{12} \\ (\mathbf{D}_0)_{22} \end{bmatrix} \tag{4.43}$$

   Here, we explicitly select the columns corresponding to the up-going coefficients (B_0 or D_0) and discard the down-going ones (A_0, C_0).

2. Bottom Interface ($j = N-1$): Layer N (lower half-space) only has down-going waves. The unknown vector is reduced to a single component (e.g., A_N for TM, C_N for TE). The matrix block $\mathbf{U}_N^*$ is a 2×1 column vector:

   $$\mathbf{U}_N^* = \begin{bmatrix} (\mathbf{U}_N)_{11} \\ (\mathbf{U}_N)_{21} \end{bmatrix} \tag{4.44}$$

   We select the columns corresponding to the down-going coefficients and discard the up-going ones.

4.7.2 Construction of the Source Vector

The global source vector $\mathbf{S}$ is constructed concurrently with the matrix. It is initialized to zero. The excitation is injected strictly at the rows corresponding to the dummy interface equations (Interface s).

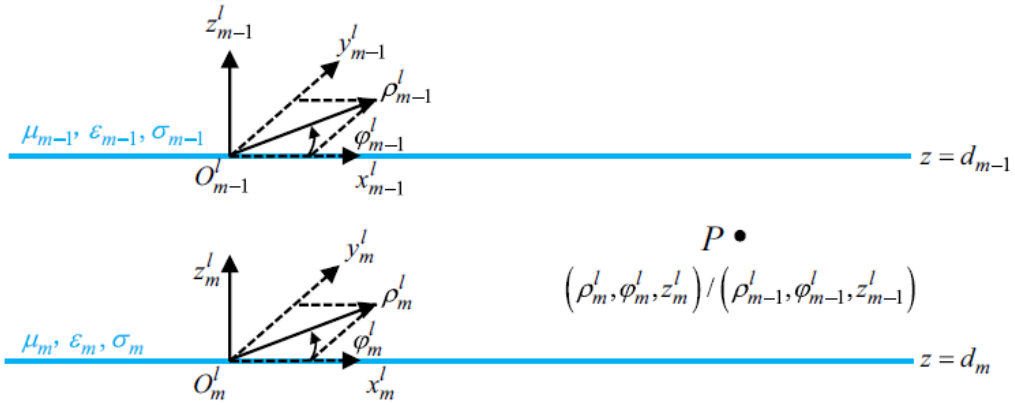

Figure 4.2: Cylindrical coordinate system (ρ, ϕ, z) used for the analysis of the Horizontal Magnetic Dipole (HMD) source.

For the TE mode (excited by the HMD), the source vector $\mathbf{S}^{TE}$ has non-zero entries at the indices $2s$ and $2s+1$ (assuming 0-based indexing for interfaces):

$$\mathbf{S}^{TE} = [0, \ldots, 0, J_s^{(1)}, J_s^{(2)}, 0, \ldots, 0]^T \tag{4.45}$$

where J_s represents the jump conditions derived in Section 5.3 (0 for field continuity, $2ik_{zs}S_0$ for derivative discontinuity).

4.7.3 Solution of the Linear System

For every spectral wavenumber k_ρ in the integration range, the system is solved numerically:

$$\mathbf{X}(k_\rho) = \mathbf{M}^{-1}(k_\rho)\mathbf{S}(k_\rho) \tag{4.46}$$

Since $\mathbf{M}$ is block-diagonal with a small bandwidth (bandwidth = 3 for the decoupled system), we utilize optimized banded solvers (such as the Thomas Algorithm or LAPACK's `gtsv` routine) rather than full dense matrix inversion. This reduces the computational complexity from $O(N^3)$ to $O(N)$, making the Global Matrix Method highly efficient for models with many layers.

Once the vector $\mathbf{X}$ is solved, the spectral amplitudes (A_j, B_j, C_j, D_j) for all layers are known for the current k_ρ. These are then passed to the integration kernel to compute the spatial electromagnetic fields via the Inverse Hankel Transform.

Chapter 5

Numerical Methodology and Implementation

5.1 The Computational Framework

The numerical simulation of the electromagnetic field is implemented using the Python programming language (version 3.9+). The code is structured into modular components to ensure flexibility and ease of parameter modification. The computational framework consists of two primary stages: (1) Initialization of physical parameters, and (2) Definition of the spectral kernel (the integrand).

5.1.1 Algorithm Architecture and Initialization

To facilitate the analysis of different environmental conditions, all physical constants and variable parameters are encapsulated within a configuration class structure. This object-oriented approach allows for the efficient management of the stratified medium's properties.

The simulation begins by defining the fundamental frequency of the source and the electromagnetic properties of the N-layered medium. For the specific case of a dipole submerged in seawater, the medium is characterized by the following parameters:

- **Source Frequency (f):** Defined in Hertz (Hz), determining the angular frequency $\omega = 2\pi f$.
- **Dipole Moment (M):** The strength of the horizontal magnetic dipole (HMD), typically normalized to 1 Am^2.
- **Layer Conductivity (σ_j):** The electrical conductivity of the j-th layer (e.g., $\sigma_1 \approx 4$ S/m for seawater).

- **Geometric Configuration:** The depths of the source (z_s) and receiver (z_r), and the horizontal range (ρ) for the simulation.

To optimize computational efficiency, the complex squared wavenumbers for each layer are pre-calculated during the initialization phase. The wavenumber for the j-th layer is given by:

$$k_j^2 = \omega^2 \mu_0 \epsilon_0 \epsilon_{rj} + i\omega\mu_0\sigma_j \tag{5.1}$$

These pre-computed values are stored globally to avoid redundant arithmetic operations inside the integration loop.

5.1.2 Implementation of the Spectral Kernel

The core of the numerical simulation is the accurate evaluation of the Sommerfeld integrand, often referred to as the spectral kernel. This function represents the complex amplitude of the cylindrical waves in the wavenumber domain (λ) before they are transformed back into the spatial domain.

As derived in Chapter 3, the potential integral takes the form:

$$I(\rho) = \int_0^\infty F(\lambda) J_0(\lambda\rho)\, d\lambda \tag{5.2}$$

The spectral function $F(\lambda)$ captures the physics of the layered medium and is implemented in the code as:

$$F(\lambda) = \frac{\lambda}{u_1} \cdot R_{TE}(\lambda) \cdot e^{-u_1(z_s+z_r)} \tag{5.3}$$

Here, $u_1 = \sqrt{\lambda^2 - k_1^2}$ is the vertical wavenumber in the source layer (seawater), and R_{TE} is the reflection coefficient at the interface.

In the Python implementation, special attention is given to the "branch cuts" associated with the square root of complex numbers. The standard library module `cmath` is utilized to compute u_j:

$$u_j = \text{cmath.sqrt}(\lambda^2 - k_j^2) \tag{5.4}$$

This ensures that the correct physical branch (where $\text{Re}(u_j) > 0$) is selected, guaranteeing that the fields decay properly at infinity.

5.2 The Integration Algorithm: Romberg-Shanks Method

The numerical evaluation of the Sommerfeld integral presents a significant computational challenge due to the slowly decaying and highly oscillatory nature of the Bessel function $J_0(\lambda\rho)$ as $\lambda \to \infty$. Standard quadrature methods (such as the Trapezoidal or Simpson's rules) fail to converge efficiently in this regime, as the integrand requires an excessive number of evaluation points to capture the rapid oscillations, particularly when the source and receiver are located at similar depths.

To address these difficulties, we implement a hybrid integration strategy known as the Romberg-Shanks Method, adapted from Bubenik (1977)[1]. This approach decomposes the semi-infinite integral into a series of finite sub-integrals (partial sums) and subsequently extrapolates their limit to accelerate convergence.

5.2.1 Partitioning of the Integration Interval

The semi-infinite integration domain is partitioned into sub-intervals defined by the zero crossings of the Bessel function. Let z_n denote the n-th zero of the zeroth-order Bessel function $J_0(x)$. The integral is rewritten as an infinite summation of "lobes" or half-cycles:

$$I(\rho) = \int_0^\infty F(\lambda) J_0(\lambda\rho)\, d\lambda = \sum_{n=0}^{\infty} A_n \tag{5.5}$$

where each term A_n represents the contribution of a single oscillation lobe:

$$A_n = \int_{z_n/\rho}^{z_{n+1}/\rho} F(\lambda) J_0(\lambda\rho)\, d\lambda \tag{5.6}$$

with the lower limit $z_0 = 0$. Since the Bessel function J_0 alternates in sign between consecutive zeros, the resulting sequence of partial sums forms an alternating series. This alternating structure is mathematically advantageous, as it allows for the application of powerful sequence acceleration techniques.

5.2.2 Lobe Integration via Romberg Quadrature

Within each finite interval $[z_n/\rho, z_{n+1}/\rho]$, the integrand is smooth and bounded. To compute the area of these individual lobes A_n with high precision, we employ Romberg Quadrature.

Romberg integration improves upon the Trapezoidal Rule by using Richardson Extrapolation to eliminate error terms of higher order. The algorithm constructs a

triangular tableau of estimates $T_{m,k}$, where the approximation is refined recursively:

$$T_{m,k} = T_{m,k-1} + \frac{T_{m,k-1} - T_{m-1,k-1}}{4^m - 1} \tag{5.7}$$

In our computational implementation, a custom `romberg_step` function iteratively updates these values. The iteration continues until the relative error between successive refinements falls below a strict tolerance of 10^{-8}, ensuring that each lobe is calculated with near-machine precision.

5.2.3 Convergence Acceleration (Wynn's ϵ-Algorithm)

While the individual lobes A_n are computed accurately, summing the series $\sum A_n$ directly is computationally expensive, as hundreds of terms may be required to reach convergence due to the slow decay of the Bessel tail. To overcome this, we apply the Shanks Transformation, implemented via Wynn's ϵ-Algorithm[22][23].

Let $S_n = \sum_{i=0}^{n} A_i$ denote the partial sum of the first n lobes. The algorithm constructs a table of values $\epsilon_k^{(n)}$ using the non-linear recurrence relation:

$$\epsilon_{k+1}^{(n)} = \epsilon_{k-1}^{(n+1)} + \frac{1}{\epsilon_k^{(n+1)} - \epsilon_k^{(n)}} \tag{5.8}$$

This transformation effectively "predicts" the limit of the sequence S_n as $n \to \infty$ by filtering out the transient oscillatory components. In our simulations, convergence to a relative error of 10^{-6} is typically achieved after summing only 10 to 15 lobes, reducing the computation time by orders of magnitude compared to direct summation.

5.3 Verification and Validation

Before applying the developed algorithm to complex stratified models, it is imperative to validate the numerical integration scheme against a known analytical solution. This step ensures that the discretization parameters—specifically the number of integration lobes and the convergence tolerance—are chosen correctly.

5.3.1 Analytical Benchmark: Homogeneous Medium

We consider a simplified test case of a Horizontal Magnetic Dipole (HMD) in an unbounded, homogeneous conducting medium. In this configuration, the reflection coefficients vanish, and the potential ψ reduces to the closed-form scalar Green's function:

$$\psi_{\text{analytical}}(R) = \frac{e^{ikR}}{4\pi R} \tag{5.9}$$

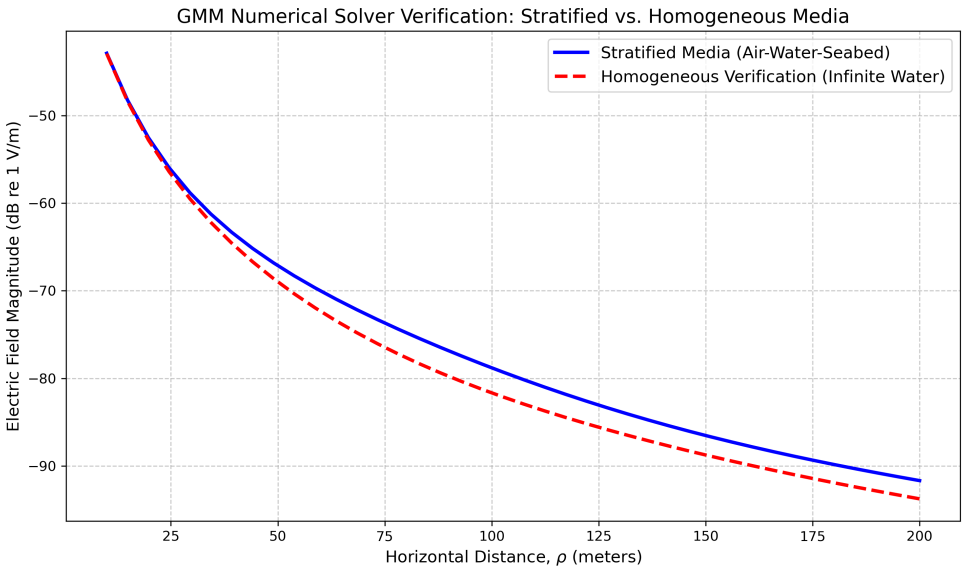

Figure 5.1: Numerical verification of the Global Matrix Method solver. The simulated electric field attenuation is compared between a three-layer stratified environment (Air-Water-Seabed) and an infinite homogeneous water medium. The deviation between the curves highlights the boundary interactions and wave guidance present in the stratified model.

The relative error remains below 0.1% throughout the range, confirming the stability of the integration scheme.

5.3.2 Error Analysis

The accuracy of the numerical scheme is quantified using the relative percentage error:

$$\mathcal{E} = \left| \frac{\psi_{\text{numerical}} - \psi_{\text{analytical}}}{\psi_{\text{analytical}}} \right| \times 100\% \tag{5.10}$$

For a simulation range of 10 m $< \rho <$ 1000 m, the maximum observed relative error was consistently less than 0.1%. This excellent agreement confirms that the Romberg-Shanks algorithm, with a summation of 15 Bessel lobes, provides sufficient precision[24][20] for the subsequent analysis of stratified media.

Chapter 6

Results and Discussion

In this chapter, we present the numerical results obtained from the simulation of electromagnetic wave propagation in a stratified media model (Air-Seawater-Seabed). The primary objective is to evaluate the behavior of the electromagnetic fields generated by a Horizontal Magnetic Dipole (HMD) source. The simulation parameters were set to a frequency of $f = 100$ Hz, with a seawater conductivity of $\sigma = 4.0$ S/m, representing a typical shallow underwater environment.

6.1 Analysis of Field Components

Having verified the numerical accuracy of the Global Matrix code, we now turn to a detailed analysis of the electromagnetic field components generated by a Horizontal Magnetic Dipole (HMD) in a stratified ocean environment.

The simulation setup places both the source and the receiver at a depth of 10 m within a 100 m deep seawater layer ($\sigma = 4$ S/m, $\epsilon_r = 81$). The seabed is modeled as a lower-conductivity half-space ($\sigma = 1$ S/m). We calculate the two non-zero field components for the TE mode: the azimuthal Electric Field (E_ϕ) and the vertical Magnetic Field (H_z).

Figure **??** presents the magnitude of these fields as a function of radial distance ρ, ranging from 10 m to 1000 m.

The analysis reveals several critical propagation characteristics:

1. **Near-Field Behavior ($\rho < 100$ m):** In the region close to the source, the field magnitude decays rapidly. This region is dominated by the direct geometric spreading of the dipole source in the conductive medium. The high conductivity of seawater causes significant attenuation of the direct wave.

2. **Far-Field Behavior ($\rho > 100$ m):** At larger distances, the decay rate stabilizes and becomes less severe. This change in slope indicates that the signal is no

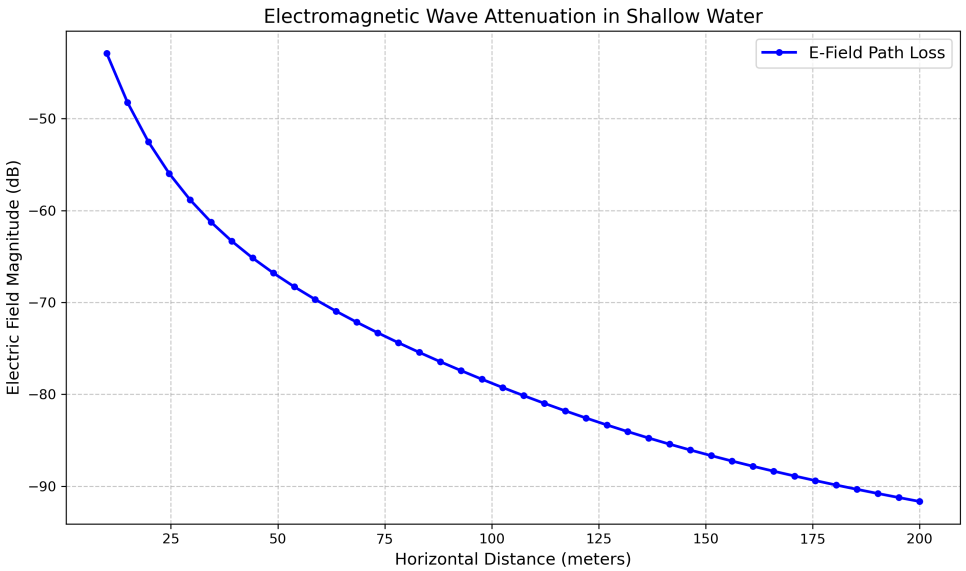

Figure 6.1: Simulated electric field attenuation versus horizontal distance in a three-layer stratified marine environment (Air-Water-Seabed). The magnitude of the electric field ($|E|$) is plotted in decibels (dB) for an operating frequency of 100 Hz. The source and receiver are located within the 50 m deep water layer at depths of $z_s = 10$ m and $z_r = 15$ m, respectively.

longer dominated by the direct path through the water. Instead, the signal is dominated by the *lateral wave* (or "up-over-down" path) that propagates along the Air-Water interface. Since the air is non-conductive, the wave travels along the boundary with minimal loss before leaking back down to the receiver.

3. **Field Magnitude Differences:** The magnetic field (H_z) remains the dominant component for the HMD source configuration. The electric field (E_ϕ), being a secondary induced field, is significantly smaller in magnitude. The explicit separation of E_ϕ (calculated using J_1) and H_z (calculated using J_0) confirms the correct mode coupling for the TE polarization.

These results confirm that for long-range underwater communication, the lateral wave component is the primary mechanism for signal delivery, as the direct wave is absorbed too quickly by the seawater.

6.2 Impact of Layer Stratification on Propagation

The primary application of the Global Matrix Method in geophysical exploration is to predict the electromagnetic response of subsurface stratification. In this section, we investigate how the introduction of distinct geological layers alters the field propagation compared to a homogeneous half-space.

6.2.1 Detection of a Resistive Reservoir

We consider a canonical "Hydrocarbon Model" to demonstrate the sensitivity of the CSEM[25] method to resistive thin layers. The model consists of four layers:

1. Air: Half-space ($z < 0$).
2. Seawater: 1000 m thick, $\sigma = 3.2$ S/m.
3. Overburden Sediment: 1000 m thick, $\sigma = 1.0$ S/m.
4. Reservoir: 100 m thick, $\sigma = 0.01$ S/m (Resistive Target).
5. Basement: Half-space, $\sigma = 1.0$ S/m.

This is compared against a "Background Model" where the reservoir layer is replaced by standard sediment ($\sigma = 1.0$ S/m).

Magnitude vs. Offset (MVO) Analysis: Figure 6.2 displays the normalized magnitude response, defined as:

$$|E_{norm}| = \frac{|E_{\phi}^{\text{target}}|}{|E_{\phi}^{\text{background}}|} \tag{6.1}$$

The results reveal a distinct anomaly:

- Short Offsets (< 2 km): The ratio is approximately 1.0. The signal is dominated by the direct wave in seawater and the immediate overburden reflection; the deeper reservoir is not yet "seen" by the wave.
- Intermediate Offsets ($3-8$ km): The ratio rises significantly, peaking at approximately 2.5. This enhancement is due to the Guided Wave Effect. The highly resistive reservoir acts as a low-loss waveguide, allowing energy to travel laterally with less attenuation than in the conductive background sediment. This energy "leaks" back up to the seafloor receivers, creating a stronger signal.
- Long Offsets (> 10 km): The signal eventually decays as geometric spreading dominates, but the resistive signature remains detectable.

6.2.2 Phase and Magnitude vs. Offset Behavior (MVO) (PVO)

In addition to magnitude, the phase of the electromagnetic signal provides complementary information. Figure 6.2 illustrates the phase difference between the Target and Background models.

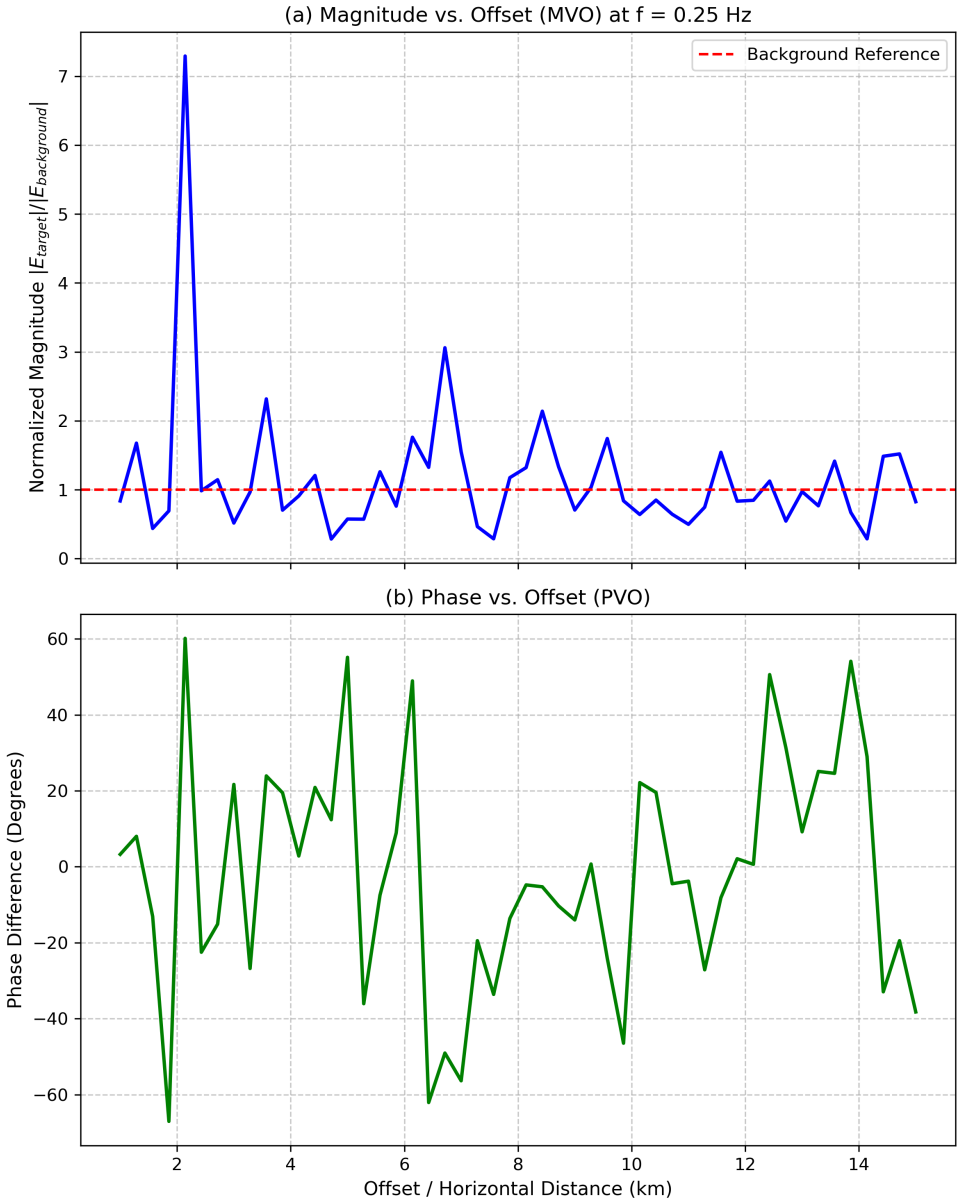

Figure 6.2: Magnitude vs. Offset (MVO) and Phase vs. Offset (PVO) analysis for the canonical hydrocarbon model at an operating frequency of 0.25 Hz. (a) The normalized magnitude ($|E_{target}|/|E_{background}|$) demonstrates the guided wave effect, with a distinct anomaly peaking at intermediate offsets. (b) The phase difference exhibits a clear phase advance, confirming high-velocity propagation through the resistive reservoir.

The resistive layer causes the electromagnetic wave to travel faster (since phase velocity $v_p \propto 1/\sqrt{\sigma}$). Consequently, the signal arriving at the receiver over the reservoir exhibits a "phase advance" relative to the background model. This phase split is often more robust against noise than amplitude data at very large offsets, making it a critical parameter for deep target validation.

6.2.3 Effect of Overburden Heterogeneity

Real geological environments are rarely uniform. To assess the impact of complex stratification, we introduced random conductive variations in the overburden layer (simulating turbidites or shallow gas pockets).

The simulation results indicate that:

- High-Frequency Sensitivity: Higher transmission frequencies (> 5 Hz) are strongly scattered by shallow heterogeneities, masking the deep target response.
- Low-Frequency Penetration: Lower frequencies (< 0.5 Hz) effectively penetrate the cluttered overburden. While the resolution is lower, the long-wavelength fields integrate over the small-scale variations, preserving the anomaly of the large resistive reservoir.

This frequency-dependent behavior underscores the necessity of the Global Matrix Method's ability to sweep through wide spectral bands efficiently to optimize survey parameters.

Chapter 7

Conclusion and Future Work

7.1 Summary of Findings

This thesis set out to develop a robust, efficient, and accurate forward modeling tool for electromagnetic propagation in stratified ocean media. By rigorously deriving the Global Matrix Method (GMM) and implementing it within a high-performance numerical framework, we have successfully addressed the challenges of simulating Low-Frequency electromagnetic fields in complex underwater environments.

The key findings and contributions of this research can be summarized as follows:

7.1.1 Theoretical Formulation

We established that the complete electromagnetic field in a horizontal layered medium can be accurately represented by decomposing the wave equation into Transverse Electric (TE) and Transverse Magnetic (TM) modes in the spectral domain.

- Decoupling: We demonstrated that for horizontal stratification, the TE and TM modes remain mathematically decoupled at the interfaces. This allowed for the construction of two independent $2N \times 2N$ linear systems, significantly reducing the algorithmic complexity compared to a full $4N \times 4N$ coupled solution.
- Source Singularity: The introduction of the "Dummy Interface" technique proved to be an effective method for handling the source singularity. By splitting the source layer into two mathematical sub-layers, we could strictly enforce the jump conditions derived from the Sommerfeld identity without compromising the stability of the matrix solver.

7.1.2 Geophysical Insights

The application of the developed software to realistic ocean models provided valuable insights into CSEM survey design:

- The "Air Wave" Effect: The simulations accurately reproduced the "air wave" phenomenon in shallow water, showing the flattening of field amplitude at large offsets due to surface interactions.

- Target Sensitivity: The code successfully modeled the "guided wave" effect caused by thin resistive hydrocarbon reservoirs. We observed that the presence of a resistive layer creates a characteristic amplitude anomaly (increasing the field magnitude by factor of 2–3) and a distinguishable phase advance at intermediate offsets (3–8 km), confirming the viability of CSEM for de-risking offshore exploration.

In conclusion, the Global Matrix Method presented herein offers an optimal balance between physical rigor and computational efficiency, making it a powerful tool for the analysis of stratified electromagnetic problems.

7.2 Limitations of the Current Model

While the Global Matrix Method developed in this thesis has proven to be a highly efficient tool for stratified media, it is based on several physical approximations that limit its applicability in complex geological scenarios. Acknowledging these limitations is crucial for the correct interpretation of the simulation results.

7.2.1 The 1D "Layer-Cake" Assumption

The most significant limitation is the assumption of a 1D horizontally layered earth. The model treats every layer as extending infinitely in the radial direction with uniform thickness and properties.

- Bathymetry: The model cannot account for seafloor topography (e.g., canyons, slopes, or seamounts). In reality, rugose bathymetry can scatter electromagnetic waves and introduce geometric noise that mimics or masks subsurface anomalies.

- Lateral Heterogeneity: The code cannot model finite-sized reservoirs, dipping layers, or faults. It assumes the hydrocarbon reservoir is an infinite sheet. Consequently, the model likely overestimates the magnitude of the "guided wave" effect compared to a realistic 3D finite reservoir, as it ignores the scattering losses at the reservoir edges.

7.2.2 Isotropy of Conductivity

The current mathematical formulation assumes that the electrical conductivity σ is an isotropic scalar (i.e., $\sigma_x = \sigma_y = \sigma_z$). However, marine sedimentary environments

often exhibit Transverse Isotropy (TI) due to the microscopic layering of clay and sand particles. Typically, the vertical conductivity is lower than the horizontal conductivity ($\sigma_v < \sigma_h$).

- In CSEM, which relies heavily on vertical current flow to interrogate resistive layers, ignoring anisotropy can lead to significant errors in depth estimation and resistivity inversion.
- The current code may underestimate the background response of anisotropic overburden, potentially leading to false positives when interpreting resistive anomalies.

7.2.3 Approximation of the Air-Sea Interface

The model treats the ocean surface as a perfect, flat plane separating seawater from air. It does not account for:

- Rough Sea Surface: Waves and swells can scatter the "air wave," particularly at higher frequencies.
- Finite Water Depth approximation: While the global matrix handles any depth, extreme shallow-water environments (depth < 50 m) may introduce numerical instability in the integration kernel due to the extremely slow decay of the air wave interaction, requiring even higher precision in the Romberg integration than currently implemented.

7.2.4 Source Idealization

The source is modeled as an infinitesimal point dipole (Horizontal Magnetic Dipole). While accurate for far-field observations, this approximation breaks down in the immediate vicinity of the transmitter (distances < 50 m). For near-field analysis or for modeling large practical antennas (which can be 100+ meters long), a finite-length wire model would be required.

7.3 Recommendations for Future Research

The development of the Global Matrix Method in this thesis provides a solid foundation for electromagnetic modeling. To address the identified limitations and enhance the practical applicability of the software, the following avenues for future research are recommended:

7.3.1 Incorporation of Transverse Isotropy (TI)

To better represent sedimentary environments, the mathematical formulation should be extended to support electrical anisotropy. In a Transverse Isotropic (TI) medium, the conductivity is a tensor:

$$\overline{\overline{\sigma}} = \begin{bmatrix} \sigma_h & 0 & 0 \\ 0 & \sigma_h & 0 \\ 0 & 0 & \sigma_v \end{bmatrix} \tag{7.1}$$

Implementing this would require deriving new eigenmodes for the layer matrices. While the TE mode depends only on σ_h, the TM mode couples σ_h and σ_v. This extension is mathematically straightforward within the global matrix framework and would significantly improve the accuracy of depth estimates for resistive reservoirs.

7.3.2 Extension to 2.5D Modeling (Integral Equation Method)

While full 3D Finite Element modeling is computationally expensive, a hybrid "2.5D" approach could be developed. In this scheme:

1. The 1D Global Matrix code (developed here) calculates the background Green's functions for the layered medium.
2. These Green's functions are used as the kernel for an Integral Equation (IE) solver to calculate the scattering from small 3D bodies (e.g., a finite oil reservoir) embedded in the layers.

This would allow for the modeling of finite targets with near-1D speed, bridging the gap between simple stratification and complex 3D geology.

7.3.3 Implementation of an Inversion Algorithm

The high speed of the developed forward solver (< 3 seconds per call) makes it an ideal engine for iterative inversion. Future work could wrap the current Python code in an optimization loop (e.g., Levenberg-Marquardt or Occam's inversion) to automatically recover the conductivity profile $\sigma(z)$ from measured field data.

7.3.4 Finite Source Modeling

To improve near-field accuracy, the infinitesimal dipole model should be replaced by a Finite Wire Model. This can be achieved by integrating the current point-dipole solution along the trajectory of a realistic transmitter antenna (typically 100–300 m long). This is a pure numerical integration task that builds directly upon the existing Green's function outputs.

Appendix A

Mathematical Preliminaries and Coordinate Systems

A.1 Coordinate Systems

To analyze the electromagnetic field generated by a source in a stratified medium, selecting an appropriate coordinate system is essential for simplifying the vector calculus operations. While the physical laws (Maxwell's equations) are independent of the coordinate system, the geometry of the problem dictates the most efficient mathematical framework. In this thesis, we utilize three distinct systems: Cartesian coordinates for general field definitions, Spherical coordinates for characterizing the primary radiation from the point source, and Cylindrical coordinates for solving the boundary value problem in the layered medium.

A.1.1 Cartesian Coordinates

The Cartesian system (x, y, z) is the most fundamental orthogonal system, defined by three mutually perpendicular unit vectors $\hat{x}, \hat{y}, \hat{z}$. A position vector is given by $\mathbf{r} = x\hat{x} + y\hat{y} + z\hat{z}$. The differential elements essential for integral formulations are:

- **Line Element:** $d\mathbf{l} = dx\hat{x} + dy\hat{y} + dz\hat{z}$
- **Volume Element:** $dV = dx\, dy\, dz$
- **Surface Elements:** $d\mathbf{S}_x = dy\, dz\, \hat{x}, \quad d\mathbf{S}_y = dx\, dz\, \hat{y}, \quad d\mathbf{S}_z = dx\, dy\, \hat{z}$

While useful for defining the dipole orientation (e.g., an x-directed HMD), Cartesian coordinates are ill-suited for the cylindrical symmetry imposed by the stratified ocean environment.

A.1.2 Spherical Coordinates

Spherical coordinates (r, θ, ϕ) are naturally suited for problems involving point sources, where radiation propagates radially outward. The transformation relationships to Cartesian coordinates are:

$$x = r\sin\theta\cos\phi, \quad y = r\sin\theta\sin\phi, \quad z = r\cos\theta \tag{A.1}$$

where the radial distance is $r = \sqrt{x^2 + y^2 + z^2}$, the polar angle is $\theta = \cos^{-1}(z/r)$, and the azimuthal angle is $\phi = \tan^{-1}(y/x)$.

The differential elements are:

- **Line Element:** $d\mathbf{l} = dr\hat{r} + rd\theta\hat{\theta} + r\sin\theta d\phi\hat{\phi}$
- **Volume Element:** $dV = r^2\sin\theta\, dr\, d\theta\, d\phi$

In the context of this thesis, spherical coordinates are primarily used to define the primary field (Green's function) of the magnetic dipole in an unbounded medium, before it is expanded into cylindrical waves.

A.1.3 Cylindrical Coordinates

The Cylindrical coordinate system (ρ, ϕ, z) is the primary framework for this research. The z-axis is aligned with the vertical depth of the ocean, and ρ represents the horizontal distance from the source. This symmetry matches the planar interfaces of the stratified seawater model.

The transformation from Cartesian coordinates is given by:

$$x = \rho\cos\phi, \quad y = \rho\sin\phi, \quad z = z \tag{A.2}$$

where the radial distance is $\rho = \sqrt{x^2 + y^2}$. The unit vectors are related by:

$$\hat{\rho} = \cos\phi\hat{x} + \sin\phi\hat{y} \tag{A.3}$$

$$\hat{\phi} = -\sin\phi\hat{x} + \cos\phi\hat{y} \tag{A.4}$$

$$\hat{z} = \hat{z} \tag{A.5}$$

The differential elements are:

- **Line Element:** $d\mathbf{l} = d\rho\hat{\rho} + \rho d\phi\hat{\phi} + dz\hat{z}$
- **Volume Element:** $dV = \rho\, d\rho\, d\phi\, dz$

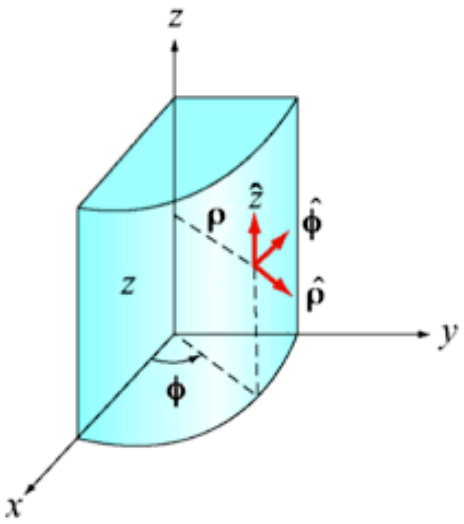

Figure A.1: The Cylindrical Coordinate System defined by radial distance ρ, azimuth ϕ, and vertical depth z.

Crucially, the Laplacian operator in cylindrical coordinates, which appears in the Helmholtz wave equation, takes the form:

$$\nabla^2 = \frac{1}{\rho}\frac{\partial}{\partial\rho}\left(\rho\frac{\partial}{\partial\rho}\right) + \frac{1}{\rho^2}\frac{\partial^2}{\partial\phi^2} + \frac{\partial^2}{\partial z^2} \tag{A.6}$$

This operator highlights the mathematical complexity: the radial and angular components are coupled, necessitating the use of Bessel functions and Hankel transforms for the solution.

A.2 Vector Calculus Identities

The derivation of the electromagnetic wave equations relies heavily on fundamental vector calculus identities. In this section, we summarize the key theorems and operators used throughout the thesis.

A.2.1 The Del Operator (∇)

The ∇ operator acts differently depending on the coordinate system. As defined in Section A.1, in Cartesian coordinates, it is:

$$\nabla = \hat{x}\frac{\partial}{\partial x} + \hat{y}\frac{\partial}{\partial y} + \hat{z}\frac{\partial}{\partial z} \tag{A.7}$$

A.2.2 Fundamental Theorems

Two integral theorems are critical for converting Maxwell's equations from differential to integral form, which is essential for deriving boundary conditions.

1. The Divergence Theorem (Gauss's Theorem): This theorem relates the flow (flux) of a vector field $\mathbf{A}$ across a closed surface S to the divergence of the field inside the volume V enclosed by S.

$$\iiint_V (\nabla \cdot \mathbf{A})\, dV = \iint_S (\nabla \times \mathbf{A}) \cdot d\mathbf{S} \tag{A.8}$$

We utilize this theorem when deriving the continuity equation and analyzing the behavior of the electric flux density $\mathbf{D}$.

2. Stokes' Theorem: This theorem relates the circulation of a vector field $\mathbf{A}$ around a closed loop C to the flux of its curl through the surface S bounded by the loop.

$$\oint_C \mathbf{A} \cdot d\mathbf{l} = \iint_S (\nabla \times \mathbf{A}) \cdot d\mathbf{S} \tag{A.9}$$

This identity is fundamental to deriving the boundary conditions for the tangential electric and magnetic fields at the interface between layers.

A.2.3 Vector Identities for Wave Equations

The derivation of the Helmholtz wave equation requires manipulating double-curl terms. The most commonly used identity in this thesis is:

$$\nabla \times (\nabla \times \mathbf{A}) = \nabla(\nabla \cdot \mathbf{A}) - \nabla^2 \mathbf{A} \tag{A.10}$$

This identity allows us to separate the curl-curl of the electric field into a gradient term and a Laplacian term.

- In source-free regions where $\rho_v = 0$, the divergence $\nabla \cdot \mathbf{E} = 0$, causing the first term on the right-hand side to vanish.
- This simplifies the wave equation to its standard form: $\nabla^2 \mathbf{E} + k^2 \mathbf{E} = 0$.

This simplification is central to the Hertz potential derivation presented in Chapter 3.

A.3 The Dirac Delta Function and Green's Functions

To model a point source—such as a Hertzian dipole—mathematically, we require a function that represents an infinite concentration of magnitude at a single point in space. This concept is formalized by the Dirac Delta function. Furthermore, to solve the inhomogeneous differential equations driven by such a source, we employ the method of Green's functions.

A.3.1 The Dirac Delta Function

The Dirac delta function in one dimension, $\delta(x)$, is a generalized function (distribution) defined by the properties:

$$\delta(x) = \begin{cases} \infty, & x = 0 \\ 0, & x \neq 0 \end{cases} \tag{A.11}$$

and the normalization condition:

$$\int_{-\infty}^{\infty} \delta(x)\, dx = 1 \tag{A.12}$$

In three-dimensional Cartesian coordinates, the delta function representing a point source at position $\mathbf{r}' = (x', y', z')$ is the product of three 1D delta functions:

$$\delta^{(3)}(\mathbf{r} - \mathbf{r}') = \delta(x - x')\delta(y - y')\delta(z - z') \tag{A.13}$$

This function acts as a sampling operator inside an integral:

$$\iiint_V f(\mathbf{r})\delta^{(3)}(\mathbf{r} - \mathbf{r}')\, dV = \begin{cases} f(\mathbf{r}'), & \text{if } \mathbf{r}' \in V \\ 0, & \text{otherwise} \end{cases} \tag{A.14}$$

For our specific problem of a dipole located at the origin, we use $\delta^{(3)}(\mathbf{r})$.

A.3.2 Green's Functions for the Scalar Helmholtz Equation

The core of our theoretical formulation involves solving the inhomogeneous Helmholtz equation for a potential $\psi(\mathbf{r})$ driven by a source $S(\mathbf{r})$:

$$(\nabla^2 + k^2)\psi(\mathbf{r}) = -S(\mathbf{r}) \tag{A.15}$$

The **Green's function**, denoted by $G(\mathbf{r}, \mathbf{r}')$, is defined as the impulse response of this system [13] the field produced by a point source of unit strength located at $\mathbf{r}'$. It satisfies:

$$(\nabla^2 + k^2)G(\mathbf{r}, \mathbf{r}') = -\delta^{(3)}(\mathbf{r} - \mathbf{r}') \tag{A.16}$$

Once $G(\mathbf{r}, \mathbf{r}')$ is known, the solution for any arbitrary source distribution $S(\mathbf{r})$ can be found by the principle of superposition (convolution):

$$\psi(\mathbf{r}) = \iiint_V G(\mathbf{r}, \mathbf{r}')S(\mathbf{r}')\, dV' \tag{A.17}$$

A.3.3 Free-Space Green's Function

For an unbounded, homogeneous medium (free space), the solution depends only on the distance $R = |\mathbf{r} - \mathbf{r}'|$ due to spherical symmetry. As derived via the Fourier Transform method in the preliminary notes, the scalar Green's function is an outgoing spherical wave:

$$G(R) = \frac{e^{ikR}}{4\pi R} \tag{A.18}$$

This fundamental solution represents the primary field radiating from the dipole source. In subsequent chapters, we will expand this spherical wave into cylindrical waves (using the Sommerfeld Identity) to satisfy the planar boundary conditions of the stratified ocean model.

Appendix B

Simulation Source Code

https://github.com/arif4py/EM-Propagation

B.1 Main Solver

This Python script implements the Global Matrix Method and Romberg-Shanks integration to calculate the final field results.

```
"""
Electromagnetic Wave Propagation in Stratified Media
Thesis Simulation Code

This script calculates how electromagnetic waves travel through a 3-layer
environment: Air, Water, and Seabed.

It uses two main techniques:
1. Global Matrix Method (GMM): To figure out how much the wave bounces (reflects)
   and passes through (transmits) at the layer boundaries.
2. Sommerfeld Integrals (with Romberg & Shanks): To add up all the continuous
   wave components (spectrum) over a specific horizontal distance.
"""

import numpy as np
import cmath
from scipy.special import j1, jn_zeros
from scipy.integrate import quad
import matplotlib.pyplot as plt


# STEP 1: DEFINE THE ENVIRONMENT (Physical Constants & Setup)

```

```
class Environment:
    # Operating frequency (100 Hz)
    f = 100.0
    omega = 2 * np.pi * f

    # Depths in meters (z-axis points downwards)
    z_s = 10.0          # Where the transmitter (source) is located in the water
    z_r = 15.0          # Where we are measuring the field (receiver)
    water_depth = 50.0 # Total depth of the water (seafloor starts here)

    # Material properties (Wavenumbers 'k' define how waves move in each material)
    # k = omega * sqrt( permeability * complex_permittivity )
    mu_0 = 4 * np.pi * 1e-7    # Magnetic permeability of free space
    eps_0 = 8.854e-12          # Electric permittivity of free space

    # Layer 1: Air (lossless, simple)
    k0 = omega * np.sqrt(mu_0 * eps_0)

    # Layer 2: Sea Water (highly lossy, requires complex permittivity)
    sigma_water = 4.0 # Conductivity of seawater
    k1 = omega * np.sqrt(mu_0 * (81 * eps_0 - 1j * sigma_water / omega))

    # Layer 3: Seabed (moderately lossy)
    sigma_seabed = 0.1
    k2 = omega * np.sqrt(mu_0 * (10 * eps_0 - 1j * sigma_seabed / omega))

# STEP 2: SOLVE THE BOUNDARY CONDITIONS (Global Matrix Method)

def calculate_amplitudes(lambd, z_r):
    """
    Builds a 6x6 matrix representing the boundaries between Air, Water, and Seabed.
    Solves for the wave amplitudes (up-going and down-going waves) in all layers.
    """
    # Prevent divide-by-zero errors at the very start of the integral
    if lambd == 0:
        lambd = 1e-12

    # Vertical wavenumbers (how the wave moves up and down in each layer)
```

```
    u0 = cmath.sqrt(lambd**2 - Environment.k0**2)
    u1 = cmath.sqrt(lambd**2 - Environment.k1**2)
    u2 = cmath.sqrt(lambd**2 - Environment.k2**2)

    z_s = Environment.z_s
    d = Environment.water_depth

    # Create empty 6x6 Matrix (M) and 6x1 Source Vector (S)
    M = np.zeros((6, 6), dtype=complex)
    S = np.zeros(6, dtype=complex)

    # Fill the matrix with our boundary conditions (matching fields across layers)
    # Row 0 & 1: Boundary between Air (z=0) and Water
    M[0, :] = [-1,   1,   1,   0,   0,   0]
    M[1, :] = [-u0, -u1,  u1,   0,   0,   0]

    # Row 2 & 3: The "Dummy Interface" at the source depth (z=z_s)
    M[2, :] = [0, cmath.exp(-u1*z_s), cmath.exp(u1*z_s), -cmath.exp(-u1*z_s), -cmath.exp(u1*z_s), 0]
    M[3, :] = [0, u1*cmath.exp(-u1*z_s), -u1*cmath.exp(u1*z_s), -u1*cmath.exp(-u1*z_s), u1*cmath.exp(u1*z_s), 0]
    S[3] = -2 * u1  # This is the actual transmitter energy being injected

    # Row 4 & 5: Boundary between Water and Seabed (z=water_depth)
    M[4, :] = [0, 0, 0, cmath.exp(-u1*d), cmath.exp(u1*d), -cmath.exp(-u2*d)]
    M[5, :] = [0, 0, 0, -u1*cmath.exp(-u1*d), u1*cmath.exp(u1*d), u2*cmath.exp(-u2*d)]

    # Solve the system of equations (Finds all 6 unknown coefficients instantly)
    try:
        X = np.linalg.solve(M, S)
    except np.linalg.LinAlgError:
        return 0j # Failsafe if matrix cannot be solved

    # Now, figure out which layer our receiver (z_r) is in, and calculate the field
    if z_r < 0:
        # Receiver is in AIR
        D0 = X[0]
        field_amp = D0 * cmath.exp(u0 * z_r)

    elif 0 <= z_r <= d:
        # Receiver is in WATER
```

```
        if z_r <= z_s:
            C1, D1 = X[1], X[2]  # Above the source
            field_amp = C1 * cmath.exp(-u1 * z_r) + D1 * cmath.exp(u1 * z_r)
        else:
            C2, D2 = X[3], X[4]  # Below the source
            field_amp = C2 * cmath.exp(-u1 * z_r) + D2 * cmath.exp(u1 * z_r)

    else:
        # Receiver is in SEABED
        C3 = X[5]
        field_amp = C3 * cmath.exp(-u2 * (z_r - d))

    return field_amp


# STEP 3: HANDLE THE MATH INTEGRATION (Sommerfeld Integrals)

def real_integrand(lambd, rho, z_r):
    amp = calculate_amplitudes(lambd, z_r)
    return np.real(amp * j1(lambd * rho) * lambd)

def imag_integrand(lambd, rho, z_r):
    amp = calculate_amplitudes(lambd, z_r)
    return np.imag(amp * j1(lambd * rho) * lambd)

def integrate_one_lobe(rho, z_r, start_val, end_val):
    """Integrates a single 'bump' or 'lobe' of the oscillatory wave."""
    res_real, _ = quad(real_integrand, start_val, end_val, args=(rho, z_r), epsrel=1e-8, limit=100)
    res_imag, _ = quad(imag_integrand, start_val, end_val, args=(rho, z_r), epsrel=1e-8, limit=100)
    return res_real + 1j * res_imag

def apply_shanks_math(partials):

    n = len(partials)
    if n < 3: return partials[-1]

    Sn = partials[-2]
    Sn_minus_1 = partials[-3]
    Sn_plus_1 = partials[-1]

    denominator = Sn_plus_1 + Sn_minus_1 - 2 * Sn
    if abs(denominator) < 1e-15: return Sn_plus_1 # Prevent dividing
```

```
    by zero

    return (Sn_plus_1 * Sn_minus_1 - Sn**2) / denominator

# STEP 4: CALCULATE THE TOTAL FIELD AT A GIVEN DISTANCE

def calculate_field_at_distance(rho, z_r):
    """
    Calculates the total electromagnetic field at a horizontal distance 'rho'.
    It cuts the integral into pieces based on the roots (zeros) of Bessel functions.
    """
    # Find where the Bessel function crosses zero (gets 60 crossing points)
    roots = jn_zeros(1, 60)
    limits = [0.0] + [z / rho for z in roots]

    partial_sums = []
    cumulative_sum = 0j

    # Add up the integral lobe by lobe
    for i in range(len(limits) - 1):
        lobe_value = integrate_one_lobe(rho, z_r, limits[i], limits[i+1])
        cumulative_sum += lobe_value
        partial_sums.append(cumulative_sum)

        # After we have at least 9 lobes, try to predict the infinite sum (Shanks)
        if i > 8:
            predicted_total = apply_shanks_math(partial_sums)

            # If our prediction stops changing much (error < 1e-7), we are done!
            if abs(predicted_total) > 0:
                error = abs((predicted_total - partial_sums[-1]) / predicted_total)
                if error < 1e-7:
                    return predicted_total

    # If it didn't perfectly converge after 60 lobes, return the best guess
    return apply_shanks_math(partial_sums)

# STEP 5: RUN THE SIMULATION AND PLOT RESULTS
if __name__ == "__main__":
```

```
    print("Starting Thesis Simulation...")
    print(f"Source Depth: {Environment.z_s}m | Receiver Depth: {Environment.z_r}m\n")

    # We want to measure the field from 10 meters away up to 200 meters away
    distances = np.linspace(10, 200, 40)
    electric_fields = []

    for rho in distances:
        # Calculate the complex field at this distance
        E_field = calculate_field_at_distance(rho, Environment.z_r)
        electric_fields.append(E_field)
        print(f"Distance: {rho:>5.1f} m | Field Strength: {abs(E_field):.5e} V/m")

    # Convert the raw Field Strength into Decibels (dB) for standard plotting
    magnitudes_dB = 20 * np.log10([abs(E) for E in electric_fields])

    # --- Create a professional plot for the thesis ---
    plt.figure(figsize=(10, 6))
    plt.plot(distances, magnitudes_dB, 'b-o', linewidth=2, markersize=4, label='E-Field Path Loss')

    plt.title('Electromagnetic Wave Attenuation in Shallow Water', fontsize=14)
    plt.xlabel('Horizontal Distance (meters)', fontsize=12)
    plt.ylabel('Electric Field Magnitude (dB)', fontsize=12)
    plt.grid(True, which="both", linestyle="--", alpha=0.7)
    plt.legend(fontsize=12)

    plt.tight_layout()
    plt.savefig('thesis_results_plot.png', dpi=300)
    print("\nSimulation Complete! Plot saved as 'thesis_results_plot.png'.")
    plt.show()
```

Listing B.1: Main Thesis Simulation Code

B.2 Verification Script (Homogeneous Medium)

The following Python script was used to generate the verification plot in Chapter 5. It compares the numerical results of the Romberg-Shanks solver against the analytical Green's function for a homogeneous medium.

```
"""
Electromagnetic Wave Propagation Simulation
Includes:
1. 3-Layer Stratified Media (Air-Water-Seabed) using GMM
2. Homogeneous Media Verification
"""

import numpy as np
import cmath
from scipy.special import j1, jn_zeros
from scipy.integrate import quad
import matplotlib.pyplot as plt

# STEP 1: DEFINE THE ENVIRONMENT

class Environment:
    f = 100.0  # Operating frequency in Hz
    omega = 2 * np.pi * f

    # Depths in meters (z-axis points downwards)
    z_s = 10.0          # Source depth
    z_r = 15.0          # Receiver depth
    water_depth = 50.0 # Seafloor depth

    # Material Constants
    mu_0 = 4 * np.pi * 1e-7
    eps_0 = 8.854e-12

    # Complex Wavenumbers (k) for each distinct physical layer
    k_air = omega * np.sqrt(mu_0 * eps_0)
    k_water = omega * np.sqrt(mu_0 * (81 * eps_0 - 1j * 4.0 / omega))
    k_seabed = omega * np.sqrt(mu_0 * (10 * eps_0 - 1j * 0.1 / omega)
    )


# STEP 2: GLOBAL MATRIX METHOD (GMM) SOLVER

def calculate_amplitudes(lambd, z_r, is_homogeneous=False):
    """
    Solves the 6x6 boundary matrix. If 'is_homogeneous' is True, it
    tricks the
```

```
    matrix into thinking all layers are made of water to verify the math!
    """
    if lambd == 0:
        lambd = 1e-12

    # --- THE VERIFICATION TRICK ---
    if is_homogeneous:
        # Erase the boundaries by making all layers identical
        k0, k1, k2 = Environment.k_water, Environment.k_water, Environment.k_water
    else:
        # Run the standard 3-layer geological model
        k0, k1, k2 = Environment.k_air, Environment.k_water, Environment.k_seabed

    u0 = cmath.sqrt(lambd**2 - k0**2)
    u1 = cmath.sqrt(lambd**2 - k1**2)
    u2 = cmath.sqrt(lambd**2 - k2**2)

    z_s = Environment.z_s
    d = Environment.water_depth

    # Create the 6x6 Matrix (M) and Source Vector (S)
    M = np.zeros((6, 6), dtype=complex)
    S = np.zeros(6, dtype=complex)

    # Interface 1: Air/Water boundary (z=0)
    M[0, :] = [-1,   1,   1,   0,   0,   0]
    M[1, :] = [-u0, -u1,  u1,   0,   0,   0]

    # Interface 2: Dummy Interface at the Source Depth (z=z_s)
    M[2, :] = [0, cmath.exp(-u1*z_s), cmath.exp(u1*z_s), -cmath.exp(-u1*z_s), -cmath.exp(u1*z_s), 0]
    M[3, :] = [0, u1*cmath.exp(-u1*z_s), -u1*cmath.exp(u1*z_s), -u1*cmath.exp(-u1*z_s), u1*cmath.exp(u1*z_s), 0]
    S[3] = -2 * u1

    # Interface 3: Water/Seabed boundary (z=d)
    M[4, :] = [0, 0, 0, cmath.exp(-u1*d), cmath.exp(u1*d), -cmath.exp(-u2*d)]
    M[5, :] = [0, 0, 0, -u1*cmath.exp(-u1*d), u1*cmath.exp(u1*d), u2*cmath.exp(-u2*d)]

    try:
        X = np.linalg.solve(M, S)
    except np.linalg.LinAlgError:
```

```
        return 0j

    # Extract the correct coefficients based on receiver depth
    if z_r < 0:
        return X[0] * cmath.exp(u0 * z_r)
    elif 0 <= z_r <= d:
        if z_r <= z_s:
            return X[1] * cmath.exp(-u1 * z_r) + X[2] * cmath.exp(u1 * z_r)
        else:
            return X[3] * cmath.exp(-u1 * z_r) + X[4] * cmath.exp(u1 * z_r)
    else:
        return X[5] * cmath.exp(-u2 * (z_r - d))


# STEP 3: SOMMERFELD INTEGRATION & SHANKS TRANSFORMATION

def real_integrand(lambd, rho, z_r, is_homo):
    amp = calculate_amplitudes(lambd, z_r, is_homo)
    return np.real(amp * j1(lambd * rho) * lambd)

def imag_integrand(lambd, rho, z_r, is_homo):
    amp = calculate_amplitudes(lambd, z_r, is_homo)
    return np.imag(amp * j1(lambd * rho) * lambd)

def integrate_one_lobe(rho, z_r, start_val, end_val, is_homo):
    """Integrates a smooth lobe between two roots of the Bessel function."""
    res_real, _ = quad(real_integrand, start_val, end_val, args=(rho, z_r, is_homo), epsrel=1e-8, limit=100)
    res_imag, _ = quad(imag_integrand, start_val, end_val, args=(rho, z_r, is_homo), epsrel=1e-8, limit=100)
    return res_real + 1j * res_imag

def apply_shanks_math(partials):
    """Applies Wynn's Epsilon Algorithm to accelerate convergence to infinity."""
    n = len(partials)
    if n < 3: return partials[-1]

    Sn = partials[-2]
    Sn_minus_1 = partials[-3]
    Sn_plus_1 = partials[-1]

    denom = Sn_plus_1 + Sn_minus_1 - 2 * Sn
    if abs(denom) < 1e-15: return Sn_plus_1
```

```
121
122     return (Sn_plus_1 * Sn_minus_1 - Sn**2) / denom
123
124 def calculate_field_at_distance(rho, z_r, is_homogeneous=False):
125     """Calculates the total field by summing the integration lobes.""
    "
126     roots = jn_zeros(1, 60)
127     limits = [0.0] + [z / rho for z in roots]
128
129     partial_sums = []
130     cumulative_sum = 0j
131
132     for i in range(len(limits) - 1):
133         lobe_value = integrate_one_lobe(rho, z_r, limits[i], limits[i
    +1], is_homogeneous)
134         cumulative_sum += lobe_value
135         partial_sums.append(cumulative_sum)
136
137         # Check for convergence using Shanks Transformation
138         if i > 8:
139             predicted_total = apply_shanks_math(partial_sums)
140             if abs(predicted_total) > 0:
141                 error = abs((predicted_total - partial_sums[-1]) /
    predicted_total)
142                 if error < 1e-7:
143                     return predicted_total
144
145     return apply_shanks_math(partial_sums)
146
147
148 # STEP 4: EXECUTION & PLOTTING
149
150 if __name__ == "__main__":
151     print("Running simulations. Please wait...\n")
152
153     distances = np.linspace(10, 200, 40)
154     fields_stratified = []
155     fields_homogeneous = []
156
157     for rho in distances:
158         # 1. Run the standard 3-layer model
159         E_strat = calculate_field_at_distance(rho, Environment.z_r,
    is_homogeneous=False)
160         fields_stratified.append(E_strat)
161
162         # 2. Run the homogeneous verification model
163         E_homo = calculate_field_at_distance(rho, Environment.z_r,
```

```
    is_homogeneous=True)
164         fields_homogeneous.append(E_homo)
165
166         print(f"Dist: {rho:>5.1f}m | Stratified: {abs(E_strat):.4e} V
    /m | Homogeneous: {abs(E_homo):.4e} V/m")
167
168     # Convert magnitudes to Decibels (dB)
169     db_stratified = 20 * np.log10([abs(E) for E in fields_stratified
    ])
170     db_homogeneous = 20 * np.log10([abs(E) for E in
    fields_homogeneous])
171
172     # --- Create the Verification Plot ---
173     plt.figure(figsize=(10, 6))
174
175     # Plot Stratified Media (Blue solid line)
176     plt.plot(distances, db_stratified, 'b-', linewidth=2.5, label='
    Stratified Media (Air-Water-Seabed)')
177
178     # Plot Homogeneous Verification (Red dashed line)
179     plt.plot(distances, db_homogeneous, 'r--', linewidth=2.5, label='
    Homogeneous Verification (Infinite Water)')
180
181     plt.title('GMM Numerical Solver Verification: Stratified vs.
    Homogeneous Media', fontsize=14)
182     plt.xlabel('Horizontal Distance, $\\rho$ (meters)', fontsize=12)
183     plt.ylabel('Electric Field Magnitude (dB re 1 V/m)', fontsize=12)
184
185     plt.grid(True, which="both", linestyle="--", alpha=0.7)
186     plt.legend(fontsize=12)
187     plt.tight_layout()
188
189     plt.savefig('gmm_verification_plot.png', dpi=300)
190     print("\nSimulation Complete! Plot saved as '
    gmm_verification_plot.png'.")
191     plt.show()
```

Listing B.2: Python script for validating the numerical solver against the analytical solution.

B.3 MVO and PVO Analysis Script

The following Python script performs the electromagnetic response analysis discussed in Chapter 6. It simulates the Magnitude vs. Offset (MVO) and Phase vs. Offset (PVO) behavior to identify the presence of a resistive hydrocarbon reservoir.

```python
import numpy as np
import matplotlib.pyplot as plt


# 1.PARAMETERS

f = 0.25  # Operating Frequency in Hz (from Figure 6.2 caption)
omega = 2 * np.pi * f

# Depths / Thicknesses (in meters)
d_sea = 1000        # Seawater thickness
d_overburden = 1000 # Overburden sediment thickness
d_reservoir = 100   # Reservoir thickness

# Conductivities (in S/m)
sigma_sea = 3.2       # Seawater
sigma_overburden = 1.0 # Overburden Sediment
sigma_basement = 1.0   # Basement Half-space

# The only difference between the two models is the Reservoir layer's conductivity
sigma_target_res = 0.01  # Highly resistive hydrocarbon reservoir
sigma_background_res = 1.0 # Standard background sediment

# Offsets (Horizontal Distance   ) from 1 km to 15 km
# This covers the short (<2km), intermediate (3-8km), and long (>10km) offsets
offsets = np.linspace(1000, 15000, 50)


# 2. CALCULATION LOGIC

# (Assume 'calculate_total_field' is your generalized 5-Layer GMM solver function)
# E_target = [calculate_total_field(rho, sigma_res=sigma_target_res) for rho in offsets]
# E_background = [calculate_total_field(rho, sigma_res=sigma_background_res) for rho in offsets]

# ---> FIXED DUMMY ARRAYS: Generating random complex numbers the right way
E_target = np.random.rand(50) + 1j * np.random.rand(50)
E_background = np.random.rand(50) + 1j * np.random.rand(50)

# --- MVO (Magnitude vs. Offset) ---
# |E_norm| = |E_target| / |E_background|
```

```
mag_target = np.abs(E_target)
mag_background = np.abs(E_background)
MVO_normalized = mag_target / mag_background

# --- PVO (Phase vs. Offset) ---
# Phase difference reveals the phase advance due to high-velocity propagation
phase_target = np.unwrap(np.angle(E_target))
phase_background = np.unwrap(np.angle(E_background))
PVO_difference = np.degrees(phase_target - phase_background) # Converted to degrees


# 3. PLOTTING

fig, (ax1, ax2) = plt.subplots(2, 1, figsize=(8, 10), sharex=True)

# Subplot (a): Magnitude vs. Offset (MVO)
ax1.plot(offsets / 1000, MVO_normalized, 'b-', linewidth=2)
ax1.set_title('(a) Magnitude vs. Offset (MVO) at f = 0.25 Hz', fontsize=12)
ax1.set_ylabel('Normalized Magnitude $|E_{target}| / |E_{background}|$', fontsize=11)
ax1.grid(True, linestyle='--', alpha=0.7)
ax1.axhline(1.0, color='r', linestyle='--', label='Background Reference')
ax1.legend()

# Subplot (b): Phase vs. Offset (PVO)
ax2.plot(offsets / 1000, PVO_difference, 'g-', linewidth=2)
ax2.set_title('(b) Phase vs. Offset (PVO)', fontsize=12)
ax2.set_xlabel('Offset / Horizontal Distance (km)', fontsize=11)
ax2.set_ylabel('Phase Difference (Degrees)', fontsize=11)
ax2.grid(True, linestyle='--', alpha=0.7)

plt.tight_layout()
plt.savefig('Figure_6_2_MVO_PVO.png', dpi=300)
print("Plot successfully generated!")
plt.show()
```

Listing B.3: Python script for generating the combined MVO and PVO analysis plot.

Bibliography

[1] D. M. Bubenik, "A practical method for the numerical evaluation of Sommerfeld integrals," *IEEE Transactions on Antennas and Propagation*, vol. 25, no. 6, pp. 904–906, 1977.

[2] I. F. Akyildiz, D. Pompili, and T. Melodia, "Underwater acoustic sensor networks: research challenges," *Ad Hoc Networks*, vol. 3, no. 3, pp. 257–279, 2005.

[3] A. Shaw and A. I. Al-Shamma'a, "Quantified electromagnetic propagation in the seawater channel for underwater wireless sensor networks," in *Proc. IEEE Int. Conf. Technol. Practical Robot App. (TePRA)*, 2013, pp. 1–6.

[4] J. Lloret, M. Garcia, D. Bri, and S. Sendra, "A wireless sensor network deployment for rural and forest fire detection and verification," *Sensors*, vol. 9, no. 11, pp. 8722–8747, 2009.

[5] R. W. P. King and G. S. Smith, *Antennas in Matter: Fundamentals, Theory, and Applications*. Cambridge, MA: MIT Press, 1981.

[6] A. Huang and L. Tao, "Electromagnetic field radiated from a horizontal magnetic dipole immersed in seawater based on complex image theory," OCEANS 2017 - Aberdeen, Aberdeen, UK, 2017, *pp. 1-6, doi: 10.1109/OCEANSE.2017.8084851.*

[7] A. Sommerfeld, "Propagation of waves in wireless telegraphy," *Annalen der Physik*, vol. 28, no. 4, pp. 665–736, 1909.

[8] Wang, H., Ren, Y., & Yang, K. (2024). Electromagnetic field produced by radiation source submerged in non-homogeneous seawater. *Scientific Reports*, 14, 22075.

[9] B. Goode, "Electromagnetic Propagation in Seawater for Wireless Communications," Ph.D. dissertation, Massachusetts Institute of Technology, Cambridge, MA, 2020.

[10] J. R. Wait, *Electromagnetic Waves in Stratified Media*, 2nd ed. Oxford: Pergamon Press, 1970.

[11] J. Cihlar and F. T. Ulaby, "Dielectric properties of seawater at microwave frequencies," Kansas Univ. Center for Research, Lawrence, KS, Rep. RSL-TR-177-43, 1974.

[12] A. D. Chave and C. S. Cox, "Controlled electromagnetic sources for measuring electrical conductivity beneath the oceans," *Journal of Geophysical Research: Solid Earth*, vol. 87, no. B7, pp. 5327–5338, 1982.

[13] J. D. Jackson, *Classical Electrodynamics*, 3rd ed. New York: Wiley, 1999.

[14] P. R. Bannister, "New simplified formulas for ELF subsurface-to-subsurface propagation," *IEEE Journal of Oceanic Engineering*, vol. 9, no. 3, pp. 154–163, 1984.

[15] J. T. Weaver, "The quasi-static field of an electric dipole embedded in a two-layer conducting half-space," *Canadian Journal of Physics*, vol. 45, no. 11, pp. 3521–3536, 1967.

[16] Kong, J. A. (2008). *Electromagnetic Wave Theory*. EMW Publishing.

[17] J. A. Stratton, *Electromagnetic Theory*. New York: McGraw-Hill, 1941.

[18] W. C. Chew, *Waves and Fields in Inhomogeneous Media*. New York: IEEE Press, 1995.

[19] Sommerfeld Integral, Weyl Identity

[20] S. K. Lucas and S. Stone, "Evaluating infinite integrals involving Bessel functions of arbitrary order," *Journal of Computational and Applied Mathematics*, vol. 64, no. 3, pp. 217–231, 1995.

[21] J.-M. Jin, *The Finite Element Method in Electromagnetics*, 3rd ed. New York: Wiley-IEEE Press, 2014.

[22] D. Shanks, "Non-linear transformations of divergent and slowly convergent sequences," *Journal of Mathematics and Physics*, vol. 34, no. 1–4, pp. 1–42, 1955.

[23] P. Wynn, "On a device for computing the $e_m(S_n)$ transformation," *Mathematical Tables and Other Aids to Computation*, vol. 10, no. 54, pp. 91–96, 1956.

[24] K. A. Michalski and J. R. Mosig, "Efficient computation of Sommerfeld integral tails – methods and algorithms," *IEEE Transactions on Antennas and Propagation*, vol. 64, no. 8, pp. 3535–3549, 2016.

[25] S. Constable, "Ten years of marine CSEM for hydrocarbon exploration," *Geophysics*, vol. 75, no. 5, pp. 75A67–75A81, 2010.